

Fast Bayesian Optimal Experimental Design for Seismic Source Inversion

Quan Long^{a,c}, Mohammad Motamed^b, Raúl Tempone^a

^a*SRI Center for Uncertainty Quantification, King Abdullah University of Science and Technology, Jeddah, Saudi Arabia*

^b*Department of Mathematics and Statistics, The University of New Mexico, USA*

^c*Institute for Computational Engineering and Sciences, The University of Texas at Austin, USA*

Abstract

We develop a fast method for optimally designing experiments in the context of statistical seismic source inversion. In particular, we efficiently compute the optimal number and locations of the receivers or seismographs. The seismic source is modeled by a point moment tensor multiplied by a time-dependent function. The parameters include the source location, moment tensor components, and start time and frequency in the time function. The forward problem is modeled by elastodynamic wave equations. We show that the Hessian of the cost functional, which is usually defined as the square of the weighted L_2 norm of the difference between the experimental data and the simulated data, is proportional to the measurement time and the number of receivers. Consequently, the posterior distribution of the parameters, in a Bayesian setting, concentrates around the “true” parameters, and we can employ Laplace approximation and speed up the estimation of the expected Kullback-Leibler divergence (expected information gain), the optimality criterion in the experimental design procedure. Since the source parameters span several magnitudes, we use a scaling matrix for efficient control of the condition number of the original Hessian matrix. We use a second-order accurate finite difference method to compute the Hessian matrix and either sparse quadrature or Monte Carlo sampling to carry out numerical integration. We demonstrate the efficiency, accuracy, and applicability of our method on a two-dimensional seismic source inversion problem.

Keywords: Bayesian experimental design, Information gain, Laplace approximation, Monte Carlo sampling, Seismic source inversion, Sparse quadrature, Uncertainty quantification

1. Introduction

In seismic source inversion, the source parameters can be estimated based on minimizing a cost functional, which is usually given by the weighted L_2 norm of the difference between the

Email addresses: quan.long@kaust.edu.sa, quan@ices.utexas.edu (Quan Long),
motamed@math.unm.edu (Mohammad Motamed), raul.tempone@kaust.edu.sa (Raúl Tempone)

recorded and simulated data. The simulated data are obtained by solving a complex forward model, which is described by a set of elastic wave equations. The recorded data are usually the time series of ground displacements, velocities and accelerations, recorded by an array of receivers (seismographs) on the surface of the ground and in observation wells. On the other hand, if we treat the source parameters as random variables, we seek a complete statistical description of all parameter values that are consistent with the noisy measured data. This can be achieved using a Bayesian approach [23] by formulating the inverse problem as a statistical inference problem, incorporating uncertainties in the measurements, the forward model, and any prior information about the parameters. The solution of this inverse problem is the set of posterior probability densities of the parameters updated from prior probability densities using Bayes theorem. Meanwhile, the maximum a posteriori (MAP) estimation is obtained by minimizing a cost functional, defined as the negative logarithm of the posterior.

Considering the financial and logistic costs of collecting real data, it is important to design an optimal data acquisition procedure, with the optimal number and locations of receivers. In the current work, we assume that there is additive Gaussian measurement noise and model the seismic source by a point moment tensor multiplied by a time-dependent function. The parameters include the source location, moment tensor components, and start time and frequency in the time function. There are in total $N_\theta = 7$ parameters in the two-dimensional model and $N_\theta = 11$ parameters in a three-dimensional model. We then consider the problem of optimal experimental design in a Bayesian framework. Under this Bayesian setting, a prior probability density function (pdf) of the source parameters is given based on expert opinion and/or historical data, and the effect of the measured data is incorporated in a likelihood function. A posterior pdf of the parameters is then obtained through Bayes theorem by the scaled product of the prior pdf and the likelihood function. To measure the amount of information obtained from a proposed experiment, we use the expected Kullback-Leibler divergence, also called the expected information gain. It is specifically defined as the marginalization of the logarithmic ratio between the posterior pdf and prior pdf over all possible values of seismic source parameters and the data. The optimal experimental setup will then be the one that maximizes the expected information gain. Finding such an optimal experiment requires calculating the expected information gains corresponding to many possible setups. See [4] for more details.

The common method for estimating the expected information gain is based on sample averages, which leads to a double-loop integral estimator [10, 20]. This approach can be prohibitively expensive when the simulated data are related to solutions of complex partial differential equations (PDEs). Hence, in such cases, such as seismic source inversion, more efficient approaches are required.

In this paper, we develop a new technique for efficiently computing the expected information gain of non-repeatable experiments arising from seismic source inversion. The efficiency of the new approach, which is based on our recent work in [12], results from the reduction of the double-loop integration to a single-loop one. This reduction can be accurately performed by Laplace approximation when the posterior distribution of the source parameters is concentrated. As the main contribution of the current work, we show that the posterior pdf concentrates around “true” source parameters, due to the fact that the

Hessian of the cost functional is proportional to the number of receivers and measurement time. Consequently, the error of our approximation diminishes by increasing the number of receivers and recording time and by improving the precision of our measurements. Hence, we extend the methodology in [12] from repeatable static problems to non-repeatable time-dependent problems of natural earthquakes. From a mathematical point of view, we seek the concentration of posterior probability distribution conditioned on a time series of data instead of repetitive experiments. We also carry out a rescaling of the original parameters to address the issue of an ill-conditioned Hessian matrix stemming from the large span of the parametric magnitudes in the seismic source term. The integrand of the approximated expected information gain is a function of the rescaled posterior covariance matrix, which can be obtained by solving $N_\theta + 2$ forward problems, consisting of $N_\theta + 1$ primal problems and 1 dual problem.

The remainder of this paper is organized in the following way. In Section 2, we formulate the experimental design problem for seismic source inversion and briefly introduce the cost functional and the expected information gain for a given experimental setup in the Bayesian setting. We present the approximated form of the expected information gain based on Laplace approximation and derive the rate of errors in Section 3. In the same section, we also summarize the finite difference method for solving the forward problems, the adjoint approach for obtaining the Hessian matrix, and the sparse quadratures and Monte Carlo sampling for numerical integration. In Section 4, we consider numerical examples for a simplified earthquake and design optimal experiments. Conclusions are presented in Section 5.

2. Experimental Design for Seismic Source Inversion

In this section, we first state the seismic source inversion problem. We then define the expected information gain in a Bayesian experimental design framework for seismic inversion.

2.1. Deterministic full waveform seismic source inversion

We first consider the full waveform seismic source inversion problem in a deterministic setting, which is stated as a PDE-constrained optimization problem. The PDEs are given by elastodynamic wave equations in a compact spatial domain, $D \subset \mathbb{R}^d$, $d = 2, 3$, with a smooth boundary, ∂D . We augment the PDE with homogeneous initial conditions and different types of boundary conditions. The initial-boundary value problem (IBVP) reads:

$$\nu(\mathbf{x}) \mathbf{u}_{tt}(t, \mathbf{x}) - \nabla \cdot \boldsymbol{\sigma}(\mathbf{u}(t, \mathbf{x})) = \mathbf{f}(t, \mathbf{x}; \boldsymbol{\theta}) \quad \text{in } [0, T] \times D, \quad (1a)$$

$$\mathbf{u}(0, \mathbf{x}) = \mathbf{0}, \quad \mathbf{u}_t(0, \mathbf{x}) = \mathbf{0} \quad \text{on } \{t = 0\} \times D, \quad (1b)$$

$$\boldsymbol{\sigma}(\mathbf{u}(t, \mathbf{x})) \cdot \hat{\mathbf{n}} = \mathbf{0} \quad \text{on } [0, T] \times \partial D_0, \quad (1c)$$

$$\mathbf{u}_t(t, \mathbf{x}) = \mathbf{B}(\mathbf{x}) \boldsymbol{\sigma}(\mathbf{u}(t, \mathbf{x})) \cdot \hat{\mathbf{n}} \quad \text{on } [0, T] \times \partial D_1. \quad (1d)$$

The IBVP solution, $\mathbf{u} = (u_1, \dots, u_d)^\top$, is the displacement field, with t and $\mathbf{x} = (x_1, \dots, x_d)^\top$ the time and location, respectively, and $\boldsymbol{\sigma}$ the stress tensor, which in the case of elastic

isotropic materials reads

$$\boldsymbol{\sigma}(\mathbf{u}) = \lambda(\mathbf{x}) \nabla \cdot \mathbf{u} I + \mu(\mathbf{x}) (\nabla \mathbf{u} + (\nabla \mathbf{u})^\top), \quad (2)$$

where I is the identity matrix. The material properties are characterized by the density, ν , and the Lamé parameters, λ and μ . Two types of boundary conditions are imposed on the boundary, ∂D : a homogeneous Neumann (stress-free) boundary condition (1c) on ∂D_0 , and an absorbing boundary condition (1d) on $\partial D_1 = \partial D \setminus \partial D_0$, where $\hat{\mathbf{n}}$ is the outward unit normal to the boundary, and \mathbf{B} is a given matrix, see for instance [5, 19]. We visualize such a compact domain together with stress-free and absorbing boundary conditions in Figure 1. The system (1) admits longitudinal (P or pressure) and transverse (S or shear) waves, which, in the case of constant density, propagate at phase velocities

$$c_p = \sqrt{(2\mu + \lambda)/\nu}, \quad c_s = \sqrt{\mu/\nu},$$

respectively. There can also be surface waves traveling along a free surface, as well as waves that travel along internal material discontinuities.

The function \mathbf{f} represents the seismic source. We consider the case of a point moment tensor source,

$$\mathbf{f}(t, \mathbf{x}; \boldsymbol{\theta}) = S(t) \mathbf{M} \nabla \delta(\mathbf{x} - \mathbf{x}_s), \quad (3)$$

located at $\mathbf{x}_s = (x_{1s}, \dots, x_{ds})^\top \in D$, where $\nabla \delta$ is the gradient of the Dirac distribution. The source time function, $S(t) = S(t; t_s, \omega_s)$, depends on two parameters: a time shift, t_s , and a frequency parameter, ω_s . The moment tensor, \mathbf{M} , is a constant symmetric matrix,

$$\mathbf{M} = \begin{pmatrix} m_{x_1 x_1} & \dots & m_{x_1 x_d} \\ \vdots & \ddots & \vdots \\ m_{x_1 x_d} & \dots & m_{x_d x_d} \end{pmatrix} \in \mathbb{R}^{d \times d}.$$

The source parameter vector, $\boldsymbol{\theta} \in \mathbb{R}^{N_\theta}$, consists of $N_\theta = \dim(\boldsymbol{\theta}) = \frac{1}{2}d^2 + \frac{3}{2}d + 2$ parameters,

$$\boldsymbol{\theta} = (x_{1s}, \dots, x_{ds}, t_s, \omega_s, m_{x_1 x_1}, \dots, m_{x_d x_d})^\top.$$

There are $N_\theta = 7$ and $N_\theta = 11$ parameters, when $d = 2$ and $d = 3$, respectively.

In the seismic source inversion problem, given $N_R \geq 2$ recorded waveforms, the goal is to find the source parameter vector, $\boldsymbol{\theta}$. This is achieved, for instance, by minimizing a full waveform cost functional, which is given by the difference between the recorded and simulated waveforms,

$$\mathcal{X}(\boldsymbol{\theta}) = \frac{1}{2} \sum_{r=1}^{N_R} \int_{t=0}^T |\mathbf{u}(t, \mathbf{x}_r) - \mathbf{d}_r(t)|^2 dt. \quad (4)$$

Here, $\mathbf{u}(t, \mathbf{x}_r)$ and $\mathbf{d}_r(t)$, with $r = 1, \dots, N_R$, are the simulated and recorded waveforms at the r -th recording station, respectively, and $|\mathbf{v}|$ denotes the magnitude of the vector, $\mathbf{v} \in \mathbb{R}^d$. In practice, the data are recorded at N_t discrete time levels $t_m \in [0, T]$, where

$0 = t_0 < t_1 < \dots < t_{N_t-2} < t_{N_t-1} = T$. Moreover, the problem (1) cannot be solved analytically and needs to be discretized. The discrete cost functional corresponding to (4) may therefore be written as

$$\mathcal{X}_d(\boldsymbol{\theta}) = \frac{1}{2} \sum_{r=1}^{N_R} \sum_{m=0}^{N_t-1} |\mathbf{u}_{\mathbf{i}_r}^m - \mathbf{d}_r(t_m)|^2, \quad (5)$$

where $\mathbf{u}_{\mathbf{i}_r}^m \approx \mathbf{u}(t_m, \mathbf{x}_r)$ is a finite difference approximate solution to (1), assuming that all recording stations coincide with grid points, i.e., $\mathbf{x}_r = \mathbf{x}_{\mathbf{i}_r}$ for some d -dimensional index vector, $\mathbf{i}_r = (i_{1r}, \dots, i_{dr})$. See Section 3.3.1 for more details on the finite difference approximation of (1).

It is to be noted that the inverse problem based on the minimization of (5) is generally an ill-posed problem when the dimension of the parameter vector N_θ is large. This means that infinitely many parameter vectors $\boldsymbol{\theta}$ match the recorded data. In such cases, in order to obtain a well-posed problem, the cost functional (5) is often augmented by additional regularizing terms. See for instance [24] for more details. Here, we focus on the case where N_θ is small compared to the number of measurements and the problem is well-posed.

The above inversion techniques are deterministic and do not take into account the uncertainty in the measurements. Therefore, in the next section, we consider a Bayesian framework that accounts for the uncertainty in the problem.

2.2. Bayesian inference and experimental design for seismic source inversion

Here, we consider the inversion and the experimental design problems in a Bayesian framework by including uncertainty in the form of additive noise in the measurements.

Let $\boldsymbol{\xi} \in \mathbb{R}^{N_e}$ be a given experimental setup, which is a vector of N_e design parameters. For instance, it may consist of the number, N_R , and the location, $\{\mathbf{x}_r\}_{r=1}^{N_R}$, of the seismographs, recording the wave forms, $\{\mathbf{d}_r(t)\}_{r=1}^{N_R}$. Moreover, let

$$\mathbf{g}_r = \mathbf{g}_r(t, \boldsymbol{\theta}, \boldsymbol{\xi}) : [0, T] \times \mathbb{R}^{N_\theta} \times \mathbb{R}^{N_e} \rightarrow \mathbb{R}^d \quad (6)$$

be a forward model for computing the vector of outputs at the r -th recording station, given a source parameter vector, $\boldsymbol{\theta}$, and an experimental setup, $\boldsymbol{\xi}$. We further assume that there is additive Gaussian measurement noise and collect N_R observation vectors,

$$\mathbf{y}_r(t) = \mathbf{g}_r(t, \boldsymbol{\theta}^*, \boldsymbol{\xi}) + \boldsymbol{\epsilon}_r, \quad \text{with } r = 1, \dots, N_R, \quad (7)$$

using the same experimental set-up, $\boldsymbol{\xi}$. Here, $\boldsymbol{\theta}^*$ is the N_θ -dimensional vector of "true" parameters used to generate N_R synthetic data, and $\boldsymbol{\epsilon}_r$ is assumed to be additive independent and identically distributed (i.i.d.) Gaussian noise, $\boldsymbol{\epsilon}_r \sim \mathcal{N}(\mathbf{0}, \mathbf{C}_\epsilon)$, corresponding to the r -th observation. Hence, the deterministic output vector, $\mathbf{g}_r(t, \boldsymbol{\theta}^*, \boldsymbol{\xi})$, is the mean of the observation vector, $\mathbf{y}_r(t)$. Moreover, the collection of N_R observed data points, $\{\mathbf{y}_r(t)\}_{r=1}^{N_R}$, is i.i.d., given specific values of t , $\boldsymbol{\theta}^*$, and $\boldsymbol{\xi}$. Note that, in practice, the observations are recorded at N_t discrete time levels, $\{t_m\}_{m=0}^{N_t-1}$.

In seismic inversion, the outputs are usually the waveforms at the recording stations obtained by discretizing the forward problem (1). We therefore consider the following parameter-to-observable map for the forward model (6):

$$\mathbf{g}_r = \mathbf{u}(t_m, \mathbf{x}_r; \boldsymbol{\theta}, \boldsymbol{\xi}), \quad \text{with } r = 1, \dots, N_R, \quad m = 0, \dots, N_t - 1, \quad (8)$$

where, we have abused the notation to emphasize the indirect dependence of $\mathbf{u}(t_m, \mathbf{x}_r)$ on $\boldsymbol{\theta}$ and $\boldsymbol{\xi}$.

The Bayes theorem gives the posterior pdf of the parameter vector as

$$p_{\boldsymbol{\Theta}}(\boldsymbol{\theta}|\{\mathbf{y}_r\}, \boldsymbol{\xi}) = \frac{p(\{\mathbf{y}_r\}|\boldsymbol{\theta}, \boldsymbol{\xi}) p_{\boldsymbol{\Theta}}(\boldsymbol{\theta})}{p(\{\mathbf{y}_r\}|\boldsymbol{\xi})}.$$

We note the fact that $p(\{\mathbf{y}_r\}|\boldsymbol{\xi})$ is a scaling factor, which does not depend on $\boldsymbol{\theta}$. The posterior of the parameter vector is proportional to the product of the likelihood function and the prior pdf,

$$p_{\boldsymbol{\Theta}}(\boldsymbol{\theta}|\{\mathbf{y}_r\}, \boldsymbol{\xi}) \propto \exp\left(-\frac{1}{2} \sum_{r=1}^{N_R} \sum_{m=0}^{N_t-1} \mathbf{r}_r(t_m, \boldsymbol{\theta}, \boldsymbol{\xi})^\top \mathbf{C}_\epsilon^{-1} \mathbf{r}_r(t_m, \boldsymbol{\theta}, \boldsymbol{\xi})\right) p_{\boldsymbol{\Theta}}(\boldsymbol{\theta}). \quad (9)$$

Here, the residual \mathbf{r}_r for the r -th measurement at the m -th time level reads

$$\mathbf{r}_r(t_m, \boldsymbol{\theta}, \boldsymbol{\xi}) := \mathbf{y}_r(t_m, \boldsymbol{\xi}) - \mathbf{g}_r(t_m, \boldsymbol{\theta}, \boldsymbol{\xi}) = \mathbf{g}_r(t_m, \boldsymbol{\theta}^*, \boldsymbol{\xi}) - \mathbf{g}_r(t_m, \boldsymbol{\theta}, \boldsymbol{\xi}) + \boldsymbol{\epsilon}_r, \quad (10)$$

where $\boldsymbol{\theta}$ is the generic unknown parameter to evaluate the posterior.

We then define a cost functional as the negative logarithm of the posterior,

$$\mathcal{L}(\boldsymbol{\theta}) := -\log(p_{\boldsymbol{\Theta}}(\boldsymbol{\theta}|\{\mathbf{y}_r\}, \boldsymbol{\xi})) = \frac{1}{2} \sum_{r=1}^{N_R} \sum_{m=0}^{N_t-1} \mathbf{r}_r(t_m, \boldsymbol{\theta}, \boldsymbol{\xi})^\top \mathbf{C}_\epsilon^{-1} \mathbf{r}_r(t_m, \boldsymbol{\theta}, \boldsymbol{\xi}) - h(\boldsymbol{\theta}) + C, \quad (11)$$

where $h(\boldsymbol{\theta}) = \log(p_{\boldsymbol{\Theta}}(\boldsymbol{\theta}))$, and C is a constant.

Maximizing the likelihood amounts to minimizing the cost functional (11). We also note the direct relation between the cost functional (11) and the cost functional (5) in the deterministic setting, where only the first term in (11) is retained and \mathbf{C}_ϵ is an identity matrix. The second term in (11) is related to the regularizing terms, which can be added to (5) to obtain a well-posed deterministic problem. Moreover, we derive our approximation of the expected information gain for a fixed value of $\boldsymbol{\xi}$, which is not treated as a variable in the rest of the paper. We also do not write it as a condition in a probability distribution for the sake of conciseness.

2.3. Expected information gain

The Kullback-Leibler divergence is a non-symmetrical measure of the distance between two probability distributions [11]. It is related to many other statistical invariants. For example, if we treat the posterior pdf as a small perturbation of the prior pdf, the Hessian

of the Kullback-Leibler divergence is the Fisher information matrix. The Kullback-Leibler divergence measures how much information the data carries about the parameter. When designing an experiment in the context of parameter inference, it is important to maximize the expected information gain.

The Kullback-Leibler (K-L) divergence for a given experiment reads

$$D_{\text{KL}}(\mathbf{y}_r) := \int_{\boldsymbol{\Theta}} \log \frac{p_{\boldsymbol{\Theta}}(\boldsymbol{\theta}|\{\mathbf{y}_r\})}{p_{\boldsymbol{\Theta}}(\boldsymbol{\theta})} p_{\boldsymbol{\Theta}}(\boldsymbol{\theta}|\{\mathbf{y}_r\}) d\boldsymbol{\theta}, \quad (12)$$

where $p_{\boldsymbol{\Theta}}(\boldsymbol{\theta})$ and $p_{\boldsymbol{\Theta}}(\boldsymbol{\theta}|\{\mathbf{y}_r\})$ are respectively the prior and posterior pdfs of the unknown random parameter, $\boldsymbol{\theta}$.

The corresponding expected K-L divergence, which represents the expected information gain in the unknown parameters, $\boldsymbol{\theta}$, is then given by:

$$I := \mathbb{E}_{\mathcal{Y}}[D_{\text{KL}}] = \int_{\mathcal{Y}} \int_{\boldsymbol{\Theta}} \log \frac{p_{\boldsymbol{\Theta}}(\boldsymbol{\theta}|\{\mathbf{y}_r\})}{p_{\boldsymbol{\Theta}}(\boldsymbol{\theta})} p_{\boldsymbol{\Theta}}(\boldsymbol{\theta}|\{\mathbf{y}_r\}) p(\{\mathbf{y}_r\}) d\boldsymbol{\theta} d\{\mathbf{y}_r\}. \quad (13)$$

As mentioned in the introduction, using the direct sample average to estimate the expected information gain leads to a double-loop summation. In the next section, we present a fast technique for computing (13) based on Laplace approximations, motivated by [12, 13].

3. Fast Estimation of Expected Information Gain

In [12], it is shown that if we are able to carry out M repetitive experiments and if M is large, the expected information gain can be estimated by Laplace approximation with a diminishing error asymptotically proportional to M^{-1} . In seismic source inversion, the large- M assumption is not fulfilled. Without losing generality, we show in this section that the error of the Laplace approximation also decreases when the number of receivers and the measurement time increase. Therefore, we can obtain a fast estimator of the expected information gain in the case of non-repeatable experiments.

We consider the cost functional, $\mathcal{L}(\boldsymbol{\theta})$, in (11) and let $\hat{\boldsymbol{\theta}}$ be its minimizer,

$$\hat{\boldsymbol{\theta}} = \arg \min_{\boldsymbol{\theta}} \mathcal{L}(\boldsymbol{\theta}). \quad (14)$$

We further make the following precise assumptions:

- *Assumption A1.* The smallest singular value of the Jacobian of the output model, $\mathbf{g}_r(t_m, \boldsymbol{\theta})$, with respect to $\boldsymbol{\theta}$ is bounded, uniformly in $\boldsymbol{\theta}$ and t , from below and away from zero by a constant.
- *Assumption A2.* The output model, $\mathbf{g}_r(t_m, \boldsymbol{\theta})$, satisfies $\mathbf{g}_r \in \mathbf{C}^2(\mathbb{R}^{N_\theta})$, $\forall t_m \in \mathbb{R}_+$.

The above two assumptions are used to estimate the magnitudes of quantities, e.g., (32), and rates of errors in the approximations, presented in Theorems 1-4 and in the appendix.

We now collect the main results of the paper in Section 3.1, followed by the proofs in Section 3.2. We then present a fast numerical method for computing the expected information gain in Section 3.3.

3.1. Main results

In this section, we state the main results. Here, we explain two notations: first, for two real vectors $\mathbf{a} = (a_1, a_2)^\top$ and $\mathbf{b} = (b_1, b_2)^\top$, we have $\nabla_{\boldsymbol{\theta}} \nabla_{\boldsymbol{\theta}} \mathbf{a} \circ \mathbf{b} = \sum_{i=1}^2 b_i \nabla_{\boldsymbol{\theta}} \nabla_{\boldsymbol{\theta}} a_i$. Second, \mathcal{O}_P denotes big-O in probability, e.g., we write $\varepsilon_N = \mathcal{O}_P(N^{-1/2})$, if and only if for a given $\epsilon > 0$, there exist a constant N_0 and an integer K , such that for all $N > N_0$, $P(|\varepsilon_N| > KN^{-1/2}) < \epsilon$.

Theorem 1. *Under assumptions A1 and A2, the minimizer (14) of the cost functional (11) is given by*

$$\hat{\boldsymbol{\theta}} = \boldsymbol{\theta}^* + \mathcal{O}_P(N^{-1/2}), \quad (15)$$

or by

$$\hat{\boldsymbol{\theta}} = \boldsymbol{\theta}^* + \mathbf{H}(\boldsymbol{\theta}^*)^{-1} \left(\sum_{r=1}^{N_R} \sum_{m=0}^{N_t-1} \boldsymbol{\epsilon}_r^\top \mathbf{C}_\epsilon^{-\top} \nabla_{\boldsymbol{\theta}} \mathbf{g}_r(t_m, \boldsymbol{\theta}^*) + \nabla_{\boldsymbol{\theta}} h(\boldsymbol{\theta}^*) \right)^\top + \mathcal{O}_P(N^{-1}), \quad (16)$$

where the total number of measurements is

$$N = N_R \times N_t,$$

and the Hessian of \mathbf{g}_r with respect to $\boldsymbol{\theta}$ is

$$\mathbf{H}(\boldsymbol{\theta}^*) = \sum_{r=1}^{N_R} \sum_{m=0}^{N_t-1} \left(\nabla_{\boldsymbol{\theta}} \mathbf{g}_r(t_m, \boldsymbol{\theta}^*)^\top \mathbf{C}_\epsilon^{-1} \nabla_{\boldsymbol{\theta}} \mathbf{g}_r(t_m, \boldsymbol{\theta}^*) - \nabla_{\boldsymbol{\theta}} \nabla_{\boldsymbol{\theta}} \mathbf{g}_r(t_m, \boldsymbol{\theta}^*) \circ \mathbf{C}_\epsilon^{-1} \boldsymbol{\epsilon}_r \right) - \nabla_{\boldsymbol{\theta}} \nabla_{\boldsymbol{\theta}} h(\boldsymbol{\theta}^*).$$

Theorem 2. *(Gaussian approximation of the posterior) The posterior pdf in (9) can be approximated by a Gaussian pdf as follows:*

$$p_{\boldsymbol{\Theta}}(\boldsymbol{\theta} | \{\mathbf{y}_r\}) = \frac{\exp\left(-\frac{1}{2} (\boldsymbol{\theta} - \hat{\boldsymbol{\theta}})^\top \mathbf{H}(\hat{\boldsymbol{\theta}}) (\boldsymbol{\theta} - \hat{\boldsymbol{\theta}})\right)}{(2\pi)^{N_{\boldsymbol{\theta}}/2} |\mathbf{H}(\hat{\boldsymbol{\theta}})|^{1/2}} \exp\left[\mathcal{O}_P(|\boldsymbol{\theta} - \hat{\boldsymbol{\theta}}|^3)\right] \quad (17)$$

$$= \tilde{p}_{\boldsymbol{\Theta}}(\boldsymbol{\theta} | \{\mathbf{y}_r\}) + \mathcal{O}_P(|\boldsymbol{\theta} - \hat{\boldsymbol{\theta}}|^3), \quad (18)$$

where

$$\mathbf{H}(\hat{\boldsymbol{\theta}}) = \mathbf{H}_1(\hat{\boldsymbol{\theta}}) + \mathbf{H}_2(\hat{\boldsymbol{\theta}}) - \nabla_{\boldsymbol{\theta}} \nabla_{\boldsymbol{\theta}} h(\hat{\boldsymbol{\theta}}), \quad (19)$$

with

$$\mathbf{H}_1(\hat{\boldsymbol{\theta}}) = \sum_{r=1}^{N_R} \sum_{m=0}^{N_t-1} \nabla_{\boldsymbol{\theta}} \mathbf{g}_r(t_m, \hat{\boldsymbol{\theta}})^\top \mathbf{C}_\epsilon^{-1} \nabla_{\boldsymbol{\theta}} \mathbf{g}_r(t_m, \hat{\boldsymbol{\theta}}) = \mathcal{O}(N), \quad (20)$$

$$\begin{aligned} \mathbf{H}_2(\hat{\boldsymbol{\theta}}) = & - \sum_{r=1}^{N_R} \sum_{m=0}^{N_t-1} \nabla_{\boldsymbol{\theta}} \nabla_{\boldsymbol{\theta}} \mathbf{g}_r(t_m, \hat{\boldsymbol{\theta}}) \circ \mathbf{C}_\epsilon^{-1} (\mathbf{g}_r(t_m, \boldsymbol{\theta}^*) - \mathbf{g}_r(t_m, \hat{\boldsymbol{\theta}})) \\ & - \sum_{r=1}^{N_R} \sum_{m=0}^{N_t-1} \nabla_{\boldsymbol{\theta}} \nabla_{\boldsymbol{\theta}} \mathbf{g}_r(t_m, \hat{\boldsymbol{\theta}}) \circ \mathbf{C}_\epsilon^{-1} \boldsymbol{\epsilon}_r = \mathcal{O}_P(N^{1/2}). \end{aligned} \quad (21)$$

Theorem 3. Under assumptions A1 and A2, the expected information gain is given by

$$I = \int_{\Theta} \int_{\mathcal{Y}} \left[-\frac{1}{2} \log((2\pi)^{N_{\theta}} |\mathbf{H}(\hat{\theta})^{-1}|) - \frac{N_{\theta}}{2} - h(\hat{\theta}) - \frac{\text{tr}(\mathbf{H}(\hat{\theta})^{-1} \nabla \nabla h(\hat{\theta}))}{2} \right] p(\{\mathbf{y}_r\}|\theta^*) d\{\mathbf{y}_r\} p(\theta^*) d\theta^* + \mathcal{O}(N^{-2}), \quad (22)$$

where $\mathbf{H}(\hat{\theta})$ is given by (19)-(21).

Theorem 4. Under assumptions A1 and A2, the expected information gain is given by

$$I = \int_{\Theta} \hat{D}_{KL}(\theta^*) p(\theta^*) d\theta^* + \mathcal{O}(N^{-1}), \quad (23)$$

with

$$\hat{D}_{KL} = -\frac{1}{2} \log((2\pi)^{N_{\theta}} |\mathbf{H}_1(\theta^*)^{-1}|) - \frac{N_{\theta}}{2} - h(\theta^*). \quad (24)$$

Here, $\mathbf{H}_1(\theta^*)$ is given by (20) with $\hat{\theta}$ replaced by θ^* , which is the “true” parameter generating the synthetic data, cf. (7)

Remark 1. The expected information gain, I , in (13) can be approximated by the integral term in (22) with an asymptotic error proportional to N^{-2} . The expected information gain can also be approximated by the integral term in (23) with an asymptotic error proportional to N^{-1} . The dimension of the integration domain in Theorem 4 is less than that in Theorem 3.

3.2. Proof of the main results

In this section, we collect the proofs of the main results.

PROOF OF THEOREM 1. We first find $\mathcal{Z}(\theta)$ so that

$$\hat{\theta} = \arg \min_{\theta} \mathcal{L}(\theta) = \arg \min_{\theta} \mathcal{Z}(\theta). \quad (25)$$

By (10) and (11), we have

$$\mathcal{L}(\theta) = \mathcal{Z}(\theta) + \frac{1}{2} \sum_{r=1}^{N_R} \sum_{m=0}^{N_t-1} \epsilon_r^{\top} \mathbf{C}_{\epsilon}^{-1} \epsilon_r + C, \quad (26)$$

where

$$\begin{aligned} \mathcal{Z}(\theta) = & \frac{1}{2} \sum_{r=1}^{N_R} \sum_{m=0}^{N_t-1} (\mathbf{g}_r(t_m, \theta^*) - \mathbf{g}_r(t_m, \theta))^{\top} \mathbf{C}_{\epsilon}^{-1} (\mathbf{g}_r(t_m, \theta^*) - \mathbf{g}_r(t_m, \theta)) + \\ & \sum_{r=1}^{N_R} \sum_{m=0}^{N_t-1} (\mathbf{g}_r(t_m, \theta^*) - \mathbf{g}_r(t_m, \theta))^{\top} \mathbf{C}_{\epsilon}^{-1} \epsilon_r - h(\theta). \end{aligned}$$

Note that the last two terms in (26) are independent of $\boldsymbol{\theta}$. We then have

$$\begin{aligned} \nabla_{\boldsymbol{\theta}} \mathcal{Z}(\boldsymbol{\theta}) = & - \sum_{r=1}^{N_R} \sum_{m=0}^{N_t-1} (\mathbf{g}_r(t_m, \boldsymbol{\theta}^*) - \mathbf{g}_r(t_m, \boldsymbol{\theta}))^\top \mathbf{C}_\epsilon^{-1} \nabla_{\boldsymbol{\theta}} \mathbf{g}_r(t_m, \boldsymbol{\theta}) - \\ & \sum_{r=1}^{N_R} \sum_{m=0}^{N_t-1} \boldsymbol{\epsilon}_r^\top \mathbf{C}_\epsilon^{-\top} \nabla_{\boldsymbol{\theta}} \mathbf{g}_r(t_m, \boldsymbol{\theta}) - \nabla_{\boldsymbol{\theta}} h(\boldsymbol{\theta}), \end{aligned} \quad (27)$$

where

$$\begin{aligned} \nabla_{\boldsymbol{\theta}} \nabla_{\boldsymbol{\theta}} \mathcal{Z}(\boldsymbol{\theta}) = & - \sum_{r=1}^{N_R} \sum_{m=0}^{N_t-1} \nabla_{\boldsymbol{\theta}} \nabla_{\boldsymbol{\theta}} \mathbf{g}_r(t_m, \boldsymbol{\theta}) \circ \mathbf{C}_\epsilon^{-1} (\mathbf{g}_r(t_m, \boldsymbol{\theta}^*) - \mathbf{g}_r(t_m, \boldsymbol{\theta})) + \\ & \sum_{r=1}^{N_R} \sum_{m=0}^{N_t-1} \nabla_{\boldsymbol{\theta}} \mathbf{g}_r(t_m, \boldsymbol{\theta})^\top \mathbf{C}_\epsilon^{-1} \nabla_{\boldsymbol{\theta}} \mathbf{g}_r(t_m, \boldsymbol{\theta}) - \\ & \sum_{r=1}^{N_R} \sum_{m=0}^{N_t-1} \nabla_{\boldsymbol{\theta}} \nabla_{\boldsymbol{\theta}} \mathbf{g}_r(t_m, \boldsymbol{\theta}) \circ \mathbf{C}_\epsilon^{-1} \boldsymbol{\epsilon}_r - \nabla_{\boldsymbol{\theta}} \nabla_{\boldsymbol{\theta}} h(\boldsymbol{\theta}). \end{aligned} \quad (28)$$

The Taylor expansion of $\nabla_{\boldsymbol{\theta}} \mathcal{Z}(\boldsymbol{\theta})$ in (27) around $\boldsymbol{\theta}^*$ reads

$$\nabla_{\boldsymbol{\theta}} \mathcal{Z}(\boldsymbol{\theta}) = \nabla_{\boldsymbol{\theta}} \mathcal{Z}(\boldsymbol{\theta}^*) + (\boldsymbol{\theta} - \boldsymbol{\theta}^*)^\top \nabla_{\boldsymbol{\theta}} \nabla_{\boldsymbol{\theta}} \mathcal{Z}(\boldsymbol{\theta}^*) + \mathcal{O}(|\boldsymbol{\theta} - \boldsymbol{\theta}^*|^2). \quad (29)$$

We now evaluate (29) at $\boldsymbol{\theta} = \hat{\boldsymbol{\theta}}$, and noting that $\nabla_{\boldsymbol{\theta}} \mathcal{Z}(\hat{\boldsymbol{\theta}}) = 0$ by (25), we write

$$\hat{\boldsymbol{\theta}} - \boldsymbol{\theta}^* = -(\nabla_{\boldsymbol{\theta}} \nabla_{\boldsymbol{\theta}} \mathcal{Z}(\boldsymbol{\theta}^*))^{-1} \nabla_{\boldsymbol{\theta}} \mathcal{Z}(\boldsymbol{\theta}^*)^\top + \mathcal{O}(|\hat{\boldsymbol{\theta}} - \boldsymbol{\theta}^*|^2). \quad (30)$$

From (27), we obtain

$$\nabla_{\boldsymbol{\theta}} \mathcal{Z}(\boldsymbol{\theta}^*) = - \sum_{r=1}^{N_R} \sum_{m=0}^{N_t-1} \boldsymbol{\epsilon}_r^\top \mathbf{C}_\epsilon^{-\top} \nabla_{\boldsymbol{\theta}} \mathbf{g}_r(t_m, \boldsymbol{\theta}^*) - \nabla_{\boldsymbol{\theta}} h(\boldsymbol{\theta}^*) = \mathcal{O}_P(N^{1/2}), \quad (31)$$

where the order, $\mathcal{O}_P(N^{1/2})$, follows Appendix A.

Moreover, from (28), we obtain

$$\begin{aligned} \nabla_{\boldsymbol{\theta}} \nabla_{\boldsymbol{\theta}} \mathcal{Z}(\boldsymbol{\theta}^*) = & \sum_{r=1}^{N_R} \sum_{m=0}^{N_t-1} \nabla_{\boldsymbol{\theta}} \mathbf{g}_r(t_m, \boldsymbol{\theta}^*)^\top \mathbf{C}_\epsilon^{-1} \nabla_{\boldsymbol{\theta}} \mathbf{g}_r(t_m, \boldsymbol{\theta}^*) - \\ & \sum_{r=1}^{N_R} \sum_{m=0}^{N_t-1} \nabla_{\boldsymbol{\theta}} \nabla_{\boldsymbol{\theta}} \mathbf{g}_r(t_m, \boldsymbol{\theta}^*) \circ \mathbf{C}_\epsilon^{-1} \boldsymbol{\epsilon}_r - \nabla_{\boldsymbol{\theta}} \nabla_{\boldsymbol{\theta}} h(\boldsymbol{\theta}^*) \\ = & \mathcal{O}(N) + \mathcal{O}_P(N^{1/2}) = \mathcal{O}_P(N), \end{aligned} \quad (32)$$

where the orders $\mathcal{O}_P(N^{1/2})$ and $\mathcal{O}(N)$ of the second and first terms in the right-hand side follow Appendices B and C, respectively. The proof is completed by (30)-(32). \square

PROOF OF THEOREM 2. Let $\tilde{\mathcal{L}}(\boldsymbol{\theta})$ be the second-order Taylor expansion of $\mathcal{L}(\boldsymbol{\theta})$ around $\hat{\boldsymbol{\theta}}$,

$$\tilde{\mathcal{L}}(\boldsymbol{\theta}) = \mathcal{L}(\hat{\boldsymbol{\theta}}) + \nabla_{\boldsymbol{\theta}} \mathcal{L}(\hat{\boldsymbol{\theta}}) (\boldsymbol{\theta} - \hat{\boldsymbol{\theta}}) + \frac{1}{2} (\boldsymbol{\theta} - \hat{\boldsymbol{\theta}})^\top \nabla_{\boldsymbol{\theta}} \nabla_{\boldsymbol{\theta}} \mathcal{L}(\hat{\boldsymbol{\theta}}) (\boldsymbol{\theta} - \hat{\boldsymbol{\theta}}).$$

The first term in the right hand side is independent of $\boldsymbol{\theta}$. Moreover, by (25), the second term is zero, since $\nabla_{\boldsymbol{\theta}} \mathcal{L}(\hat{\boldsymbol{\theta}}) = 0$. We are therefore left only with the third term. Similar to the proof of Theorem 1, (19) follows easily. Furthermore, the growth order in (20) follows in a similar way to Appendix C. It is left to show (21). By (10), and similar to the proof of Theorem 1, we write

$$\begin{aligned} \mathbf{H}_2(\hat{\boldsymbol{\theta}}) = & - \sum_{r=1}^{N_R} \sum_{m=0}^{N_t-1} \nabla_{\boldsymbol{\theta}} \nabla_{\boldsymbol{\theta}} \mathbf{g}_r(t_m, \hat{\boldsymbol{\theta}}) \circ \mathbf{C}_{\epsilon}^{-1} \boldsymbol{\epsilon}_r - \\ & \sum_{r=1}^{N_R} \sum_{m=0}^{N_t-1} \nabla_{\boldsymbol{\theta}} \nabla_{\boldsymbol{\theta}} \mathbf{g}_r(t_m, \hat{\boldsymbol{\theta}}) \circ \mathbf{C}_{\epsilon}^{-1} (\mathbf{g}_r(t_m, \boldsymbol{\theta}^*) - \mathbf{g}_r(t_m, \hat{\boldsymbol{\theta}})). \end{aligned} \quad (33)$$

The first term in the right-hand side of (33) is of order $\mathcal{O}_P(N^{1/2})$, similar to Appendix B. For the second term in the right-hand side of (33), we use Taylor expansion and write

$$\mathbf{g}_r(t_m, \boldsymbol{\theta}) = \mathbf{g}_r(t_m, \boldsymbol{\theta}^*) + \nabla_{\boldsymbol{\theta}} \mathbf{g}_r(t_m, \boldsymbol{\theta}^*) (\boldsymbol{\theta} - \boldsymbol{\theta}^*) + \mathcal{O}(|\boldsymbol{\theta} - \boldsymbol{\theta}^*|^2).$$

Then at $\boldsymbol{\theta} = \hat{\boldsymbol{\theta}}$, using (15), we have

$$\mathbf{g}_r(t_m, \hat{\boldsymbol{\theta}}) - \mathbf{g}_r(t_m, \boldsymbol{\theta}^*) = \mathcal{O}_P(N^{-1/2}).$$

The first term in the right-hand side of (33) dominates, and this completes the proof. \square

PROOF OF THEOREM 3. We first rewrite the information gain (12) as

$$\begin{aligned} D_{KL} = & \int_{\boldsymbol{\Theta}} \log \left(\frac{p_{\boldsymbol{\Theta}}(\boldsymbol{\theta}|\{\mathbf{y}_r\})}{p_{\boldsymbol{\Theta}}(\boldsymbol{\theta})} \right) \tilde{p}_{\boldsymbol{\Theta}}(\boldsymbol{\theta}|\{\mathbf{y}_r\}) d\boldsymbol{\theta} + \\ & \int_{\boldsymbol{\Theta}} \log \left(\frac{p_{\boldsymbol{\Theta}}(\boldsymbol{\theta}|\{\mathbf{y}_r\})}{p_{\boldsymbol{\Theta}}(\boldsymbol{\theta})} \right) (p_{\boldsymbol{\Theta}}(\boldsymbol{\theta}|\{\mathbf{y}_r\}) - \tilde{p}_{\boldsymbol{\Theta}}(\boldsymbol{\theta}|\{\mathbf{y}_r\})) d\boldsymbol{\theta}, \end{aligned}$$

where \tilde{p} is the Gaussian approximation of the posterior, p , given in Theorem 2 by (17). Then, we can write

$$D_{KL} = D_1 + D_2 + D_3 + D_4, \quad (34)$$

where

$$D_1 := \int_{\boldsymbol{\Theta}} \log(\tilde{p}_{\boldsymbol{\Theta}}(\boldsymbol{\theta}|\{\mathbf{y}_r\})) \tilde{p}_{\boldsymbol{\Theta}}(\boldsymbol{\theta}|\{\mathbf{y}_r\}) d\boldsymbol{\theta}, \quad (35)$$

$$D_2 := - \int_{\boldsymbol{\Theta}} \log(p_{\boldsymbol{\Theta}}(\boldsymbol{\theta})) \tilde{p}_{\boldsymbol{\Theta}}(\boldsymbol{\theta}|\{\mathbf{y}_r\}) d\boldsymbol{\theta} = - \int_{\boldsymbol{\Theta}} h(\boldsymbol{\theta}) \tilde{p}_{\boldsymbol{\Theta}}(\boldsymbol{\theta}|\{\mathbf{y}_r\}) d\boldsymbol{\theta}, \quad (36)$$

$$D_3 := \int_{\boldsymbol{\Theta}} \log \left(\frac{p_{\boldsymbol{\Theta}}(\boldsymbol{\theta}|\{\mathbf{y}_r\})}{\tilde{p}_{\boldsymbol{\Theta}}(\boldsymbol{\theta}|\{\mathbf{y}_r\})} \right) \tilde{p}_{\boldsymbol{\Theta}}(\boldsymbol{\theta}|\{\mathbf{y}_r\}) d\boldsymbol{\theta}, \quad (37)$$

$$D_4 := \int_{\boldsymbol{\Theta}} \log \left(\frac{p_{\boldsymbol{\Theta}}(\boldsymbol{\theta}|\{\mathbf{y}_r\})}{p_{\boldsymbol{\Theta}}(\boldsymbol{\theta})} \right) (p_{\boldsymbol{\Theta}}(\boldsymbol{\theta}|\{\mathbf{y}_r\}) - \tilde{p}_{\boldsymbol{\Theta}}(\boldsymbol{\theta}|\{\mathbf{y}_r\})) d\boldsymbol{\theta}. \quad (38)$$

The first term (35) reads

$$D_1 = -\frac{1}{2} \log((2\pi)^{N_\theta} |\tilde{\mathbf{C}}|) - \frac{N_\theta}{2}, \quad \tilde{\mathbf{C}} := \mathbf{H}(\hat{\boldsymbol{\theta}})^{-1}. \quad (39)$$

For the second term (36), we first Taylor expand $h(\boldsymbol{\theta}) = \log(p_{\boldsymbol{\Theta}}(\boldsymbol{\theta}))$ about $\hat{\boldsymbol{\theta}}$ to obtain

$$h(\boldsymbol{\theta}) = \sum_{|\boldsymbol{\alpha}| \leq 4} \frac{D^{\boldsymbol{\alpha}} h(\hat{\boldsymbol{\theta}})}{\boldsymbol{\alpha}!} (\boldsymbol{\theta} - \hat{\boldsymbol{\theta}})^{\boldsymbol{\alpha}} + \mathcal{O}_P(|\boldsymbol{\theta} - \hat{\boldsymbol{\theta}}|^5),$$

where $\boldsymbol{\alpha} \in \mathbb{N}^{N_\theta}$ is a multi-index with the following properties:

$$|\boldsymbol{\alpha}| = \sum_{i=1}^{N_\theta} \alpha_i, \quad \boldsymbol{\alpha}! = \prod_{i=1}^{N_\theta} \alpha_i!, \quad (\boldsymbol{\theta})^{\boldsymbol{\alpha}} = \prod_{i=1}^{N_\theta} \theta_i^{\alpha_i}.$$

The odd central moments of the multivariate Gaussian, \tilde{p} , in (17) are zero, and the parameter posterior covariance, $\tilde{\mathbf{C}}$, is of order $\mathcal{O}_P(N^{-1})$, due to Theorem 2. Moreover, the fourth central moment of this multivariate Gaussian is a quadratic form of the second moment, and hence is of order $\mathcal{O}_P(N^{-2})$. Consequently, we have

$$\begin{aligned} D_2 &= - \int_{\boldsymbol{\Theta}} \left[\sum_{|\boldsymbol{\alpha}| \leq 4} \frac{D^{\boldsymbol{\alpha}} h(\hat{\boldsymbol{\theta}})}{\boldsymbol{\alpha}!} (\boldsymbol{\theta} - \hat{\boldsymbol{\theta}})^{\boldsymbol{\alpha}} + \mathcal{O}_P(|\boldsymbol{\theta} - \hat{\boldsymbol{\theta}}|^5) \right] \tilde{p}(\boldsymbol{\theta}|\{\mathbf{y}_r\}) d\boldsymbol{\theta} \\ &= -h(\hat{\boldsymbol{\theta}}) - \frac{\tilde{\mathbf{C}} : \nabla \nabla h(\hat{\boldsymbol{\theta}})}{2} + \mathcal{O}_P(N^{-2}). \end{aligned} \quad (40)$$

Here, $\mathbf{A} : \mathbf{B} = \sum_{i,j} A_{ij} B_{ij}$ is the component-wise inner product of two matrices, $\mathbf{A} = (A_{ij})$ and $\mathbf{B} = (B_{ij})$ of the same size.

Next, we consider the third term (37). Since the approximate posterior, \tilde{p} , is a second-order Taylor approximation of the log posterior, p , we have

$$\log \left(\frac{p_{\boldsymbol{\Theta}}(\boldsymbol{\theta}|\{\mathbf{y}_r\})}{\tilde{p}_{\boldsymbol{\Theta}}(\boldsymbol{\theta}|\{\mathbf{y}_r\})} \right) = \sum_{|\boldsymbol{\alpha}|=3} \frac{D^{\boldsymbol{\alpha}} h_p(\hat{\boldsymbol{\theta}})}{\boldsymbol{\alpha}!} (\boldsymbol{\theta} - \hat{\boldsymbol{\theta}})^{\boldsymbol{\alpha}} + \mathcal{O}_P(|\boldsymbol{\theta} - \hat{\boldsymbol{\theta}}|^4),$$

where $h_p = \log(p_{\boldsymbol{\Theta}}(\boldsymbol{\theta}|\{\mathbf{y}_r\}))$. Similar to the analysis of the second term, D_2 , we can easily show that

$$D_3 = \mathcal{O}_P(N^{-2}). \quad (41)$$

Finally, for the fourth term (38), we have

$$\begin{aligned} D_4 &= \int_{\boldsymbol{\Theta}} \log \left(\frac{p_{\boldsymbol{\Theta}}(\boldsymbol{\theta}|\{\mathbf{y}_r\})}{p_{\boldsymbol{\Theta}}(\boldsymbol{\theta})} \right) \\ &\quad \left\{ \exp \left[\sum_{|\boldsymbol{\alpha}|=3} \frac{D^{\boldsymbol{\alpha}} h_p(\hat{\boldsymbol{\theta}})}{\boldsymbol{\alpha}!} (\boldsymbol{\theta} - \hat{\boldsymbol{\theta}})^{\boldsymbol{\alpha}} + \mathcal{O}_P(|\boldsymbol{\theta} - \hat{\boldsymbol{\theta}}|^4) \right] - 1 \right\} \tilde{p}_{\boldsymbol{\Theta}}(\boldsymbol{\theta}|\{\mathbf{y}_r\}) d\boldsymbol{\theta}. \end{aligned}$$

After the first-order Taylor expansion of the exponential term, we obtain

$$D4 = \int_{\Theta} \log \left(\frac{p_{\Theta}(\boldsymbol{\theta}|\{\mathbf{y}_r\})}{p_{\Theta}(\hat{\boldsymbol{\theta}})} \right) \left\{ \sum_{|\alpha|=3} \frac{D^{\alpha} h_p(\hat{\boldsymbol{\theta}})}{\alpha!} (\boldsymbol{\theta} - \hat{\boldsymbol{\theta}})^{\alpha} + \mathcal{O}_P(|\boldsymbol{\theta} - \hat{\boldsymbol{\theta}}|^4) \right\} \tilde{p}_{\Theta}(\boldsymbol{\theta}|\{\mathbf{y}_r\}) d\boldsymbol{\theta}.$$

Since $\log \left(\frac{p_{\Theta}(\hat{\boldsymbol{\theta}}|\{\mathbf{y}_r\})}{p_{\Theta}(\hat{\boldsymbol{\theta}})} \right)$ is asymptotically $\mathcal{O}_P(\log(N))$, and the third moment of a multivariate Gaussian is zero, we have

$$D4 = \int_{\Theta} \log \left(\frac{p_{\Theta}(\boldsymbol{\theta}|\{\mathbf{y}_r\})}{p_{\Theta}(\hat{\boldsymbol{\theta}})} \right) \mathcal{O}_P(|\boldsymbol{\theta} - \hat{\boldsymbol{\theta}}|^4) \tilde{p}_{\Theta}(\boldsymbol{\theta}|\{\mathbf{y}_r\}) d\boldsymbol{\theta} = \mathcal{O}_P(N^{-2} \log(N)). \quad (42)$$

This is the fourth moment of the Gaussian posterior, \tilde{p} , which has already been shown to be inversely proportional to N^2 .

Substituting (39)-(42) into (34), we obtain

$$D_{KL} = -\frac{1}{2} \log((2\pi)^{N_{\theta}} |\tilde{\mathbf{C}}|) - \frac{N_{\theta}}{2} + h(\hat{\boldsymbol{\theta}}) + \frac{\tilde{\mathbf{C}} : \nabla \nabla h(\hat{\boldsymbol{\theta}})}{2} + \mathcal{O}_P(N^{-2} \log(N)). \quad (43)$$

After marginalization over data, and conditioning on the “true” parameter, which has a pdf identical to the prior of the unknown parameters, the approximation and error estimation for the expected information gain (22) is obtained. This completes the proof. \square

PROOF OF THEOREM 4. Using Woodbury’s formula [8] to invert (19), we have

$$\begin{aligned} \mathbf{H}(\hat{\boldsymbol{\theta}})^{-1} &= \left[\mathbf{H}_1(\hat{\boldsymbol{\theta}}) + \mathbf{H}_2(\hat{\boldsymbol{\theta}}) - \nabla_{\boldsymbol{\theta}} \nabla_{\boldsymbol{\theta}} h(\hat{\boldsymbol{\theta}}) \right]^{-1} \\ &= \mathbf{H}_1(\hat{\boldsymbol{\theta}})^{-1} + \mathbf{H}_1(\hat{\boldsymbol{\theta}})^{-1} \mathbf{L} (\boldsymbol{\Lambda}^{-1} + \mathbf{R} \mathbf{H}_1(\hat{\boldsymbol{\theta}})^{-1} \mathbf{L})^{-1} \mathbf{R} \mathbf{H}_1(\hat{\boldsymbol{\theta}})^{-1} \end{aligned} \quad (44)$$

with $\mathbf{H}_2(\hat{\boldsymbol{\theta}}) - \nabla_{\boldsymbol{\theta}} \nabla_{\boldsymbol{\theta}} h(\hat{\boldsymbol{\theta}}) = \mathbf{L} \boldsymbol{\Lambda} \mathbf{R}$ the corresponding eigenvalue decomposition. The second term on the right-hand side of (44) is of order $\mathcal{O}_P(N^{-\frac{3}{2}})$. Hence,

$$\mathbf{H}(\hat{\boldsymbol{\theta}})^{-1} = \mathbf{H}_1(\hat{\boldsymbol{\theta}})^{-1} + \mathcal{O}_P(N^{-\frac{3}{2}}).$$

We therefore can approximate the information gain, D_{KL} , in (43) by

$$D_{KL} = \hat{D}_{KL} + \mathcal{O}_P(N^{-\frac{3}{2}}),$$

where

$$\hat{D}_{KL} := -\frac{1}{2} \log((2\pi)^{N_{\theta}} |\mathbf{H}_1(\hat{\boldsymbol{\theta}})^{-1}|) - \frac{N_{\theta}}{2} + h(\hat{\boldsymbol{\theta}}) + \frac{\mathbf{H}_1(\hat{\boldsymbol{\theta}})^{-1} : \nabla \nabla h(\hat{\boldsymbol{\theta}})}{2}.$$

Next, we Taylor expand \hat{D}_{KL} about $\boldsymbol{\theta}^*$,

$$\hat{D}_{KL}(\hat{\boldsymbol{\theta}}) = \hat{D}_{KL}(\boldsymbol{\theta}^*) + \nabla \hat{D}_{KL}(\boldsymbol{\theta}^*)^T (\hat{\boldsymbol{\theta}} - \boldsymbol{\theta}^*) + \mathcal{O}_P(|\hat{\boldsymbol{\theta}} - \boldsymbol{\theta}^*|^2) \quad (45)$$

Now, by rearranging the expected information gain, we get

$$I = \int_{\Theta} \hat{D}_{KL}(\boldsymbol{\theta}^*) p(\boldsymbol{\theta}^*) d\boldsymbol{\theta}^* + \int_{\Theta} \int_{\{\boldsymbol{\epsilon}_r\}} \nabla \hat{D}_{KL}(\boldsymbol{\theta}^*)^T (\hat{\boldsymbol{\theta}} - \boldsymbol{\theta}^*) d\boldsymbol{\theta}^* p(\{\boldsymbol{\epsilon}_r\}) d\{\boldsymbol{\epsilon}_r\} + \mathcal{O}(N^{-1}). \quad (46)$$

By Theorem 1, as $N \rightarrow \infty$, the difference, $\hat{\boldsymbol{\theta}} - \boldsymbol{\theta}^*$, is asymptotically proportional to $\boldsymbol{\epsilon}_r$ (see (16)); in other words, $\sum_{r=1}^{N_R} \sum_{m=0}^{N_t-1} \boldsymbol{\epsilon}_r^\top \mathbf{C}_\epsilon^{-\top} \nabla_{\boldsymbol{\theta}} \mathbf{g}_r(t_m, \boldsymbol{\theta}^*) = \mathcal{O}_P(N^{1/2})$ is dominant over $\nabla_{\boldsymbol{\theta}} h(\boldsymbol{\theta}^*) = \mathcal{O}(1)$, and $\mathbf{H}(\hat{\boldsymbol{\theta}})$ is dominated by its deterministic component, $\mathbf{H}_1(\hat{\boldsymbol{\theta}})$ (see Theorem 2). Since $\boldsymbol{\epsilon}_r$ is a centered Gaussian random vector, the second integral on the right-hand side of (46) vanishes. Therefore, the approximated expected information gain as shown in (46) has an error of order N^{-1} , and the proof is complete. \square

3.3. Fast numerical approach

3.3.1. Finite difference approximation of the problem

Consider a rectangular spatial domain, $D = [-L_1, L_1] \times [-L_2, 0]$, in \mathbb{R}^2 . We employ a second-order accurate finite difference scheme, proposed in [16], for solving (1). Let $h = 2L_1/(N_1 - 1) = L_2/(N_2 - 1) > 0$ denotes the spatial grid-length, where N_1 and N_2 are the numbers of grid points in the x_1 and x_2 directions, respectively. Let $\mathbf{i} = (i, j)$, and for $i = 1, \dots, N_1$ and $j = 1, \dots, N_2$, consider the computational grid

$$\mathbf{x}_{\mathbf{i}} = (x_{1i}, x_{2j}) = (-L_1 + (i - 1)h, -L_2 + (j - 1)h).$$

Denote by $\mathbf{u}_{\mathbf{i}}(t) = (u_{1i}(t), u_{2i}(t))^\top$ the semi-discrete approximation of $\mathbf{u}(t, \mathbf{x}_{\mathbf{i}})$. For interior grid points and grid points on the free surface boundary ($\partial D_0 = \{\mathbf{x} : x_1 \in [-L_1, L_1], x_2 = 0\}$), we have

$$\nu(\mathbf{x}_{\mathbf{i}}) \ddot{\mathbf{u}}_{\mathbf{i}}(t) = \mathcal{A}_h(\mathbf{u}_{\mathbf{i}}(t)) + \tilde{\mathbf{f}}(t, \mathbf{x}_{\mathbf{i}}; \boldsymbol{\theta}), \quad \mathbf{x}_{\mathbf{i}} \in D \setminus \partial D_1, \quad (47)$$

where $\tilde{\mathbf{f}}(t, \mathbf{x}_{\mathbf{i}}; \boldsymbol{\theta})$ is a discretization of the singular source term, $\mathbf{f}(t, \mathbf{x}; \boldsymbol{\theta})$, and \mathcal{A}_h is a difference operator containing standard operators D_- , D_+ , D_0 in both spatial directions and λ , μ , and h , see [16]. On the boundary, ∂D_1 , we discretize the boundary condition (1d),

$$\dot{\mathbf{u}}_{\mathbf{i}}(t) = \mathcal{B}_h(\mathbf{u}_{\mathbf{i}}(t)), \quad \mathbf{x}_{\mathbf{i}} \in \partial D_1, \quad (48)$$

where \mathcal{B}_h is a difference operator containing D_- , D_+ , ν , λ , μ , and h .

We further collect the semi-discrete solution, $\mathbf{u}_{\mathbf{i}}(t)$, at all $N_h = N_1 \times N_2$ grid points in two N_h -vectors, $\tilde{u}_1(t)$ and $\tilde{u}_2(t)$. We also collect $\tilde{\mathbf{f}}(t, \mathbf{x}_{\mathbf{i}}; \boldsymbol{\theta})$ at all N_h grid points in two N_h -vectors, $\tilde{f}_1(t; \boldsymbol{\theta})$ and $\tilde{f}_2(t; \boldsymbol{\theta})$. We finally combine the semi-discrete formulas, (47) and (48), and write them in matrix form:

$$\begin{aligned} I_1 \ddot{\tilde{u}}_1(t) + I_2 \dot{\tilde{u}}_1(t) &= A_1 \tilde{u}_1(t) + A_2 \tilde{u}_2(t) + C \tilde{f}_1(t; \boldsymbol{\theta}), \\ I_1 \ddot{\tilde{u}}_2(t) + I_2 \dot{\tilde{u}}_2(t) &= B_1 \tilde{u}_1(t) + B_2 \tilde{u}_2(t) + C \tilde{f}_2(t; \boldsymbol{\theta}). \end{aligned}$$

Here, all matrices, $A_1, A_2, B_1, B_2, C, I_1, I_2$, are in $\mathbb{R}^{N_h \times N_h}$, and $I_1 + I_2 = I$.

The full discretization is obtained by discretizing the time domain $[0, T]$ into N_t equidistant time levels, $t_m \in [0, T]$, where $0 = t_0 < t_1 < \dots < t_{N_t-2} < t_{N_t-1} = T$ with a time step

$\Delta t = T/(N_t - 1)$. We let \tilde{u}_1^m and \tilde{u}_2^m denote the full-discrete vectors, $\tilde{u}_1(t_m)$ and $\tilde{u}_2(t_m)$, respectively, and use the following central difference formulas:

$$\ddot{u}_k^m = \frac{\tilde{u}_k^{m+1} - 2\tilde{u}_k^m + \tilde{u}_k^{m-1}}{\Delta t^2}, \quad \dot{u}_k^m = \frac{\tilde{u}_k^{m+1} - \tilde{u}_k^{m-1}}{2\Delta t}, \quad k = 1, 2. \quad (49)$$

We finally arrive at the full-discrete formulas

$$U_{1\text{FD}} \equiv I_1 \frac{\tilde{u}_1^{m+1} - 2\tilde{u}_1^m + \tilde{u}_1^{m-1}}{\Delta t^2} + I_2 \frac{\tilde{u}_1^{m+1} - \tilde{u}_1^{m-1}}{2\Delta t} - A_1 \tilde{u}_1^m - A_2 \tilde{u}_2^m - C \tilde{f}_1^m = 0, \quad (50a)$$

$$U_{2\text{FD}} \equiv I_1 \frac{\tilde{u}_2^{m+1} - 2\tilde{u}_2^m + \tilde{u}_2^{m-1}}{\Delta t^2} + I_2 \frac{\tilde{u}_2^{m+1} - \tilde{u}_2^{m-1}}{2\Delta t} - B_1 \tilde{u}_1^m - B_2 \tilde{u}_2^m - C \tilde{f}_2^m = 0, \quad (50b)$$

where $\tilde{f}_k^m = \tilde{f}_k(t_m; \boldsymbol{\theta})$ with $k = 1, 2$.

3.3.2. Computation of the Hessian of cost functional

In this section, we describe in detail how to compute the Hessian, $\nabla_{\boldsymbol{\theta}} \nabla_{\boldsymbol{\theta}} \mathcal{L}$, of the cost functional, \mathcal{L} , given in (11). We consider the first term in the right-hand side of (11) and write

$$\mathcal{L}_1(\boldsymbol{\theta}) = \sum_{m=0}^{N_t-1} \mathbb{L}(t_m, \tilde{u}_1^m(\boldsymbol{\theta}), \tilde{u}_2^m(\boldsymbol{\theta})), \quad \mathbb{L} := \frac{1}{2} \sum_{r=1}^{N_R} \mathbf{r}_r(t_m, \boldsymbol{\theta})^\top \mathbf{C}_\epsilon^{-1} \mathbf{r}_r(t_m, \boldsymbol{\theta}), \quad (51)$$

where the residual \mathbf{r}_r , given in (10), is a function of \tilde{u}_1 and \tilde{u}_2 , which are in turn functions of t_m and $\boldsymbol{\theta}$. The Hessian of the remaining terms in the right-hand side of (11), i.e. $-h(\boldsymbol{\theta}) + C$, is simply $-\nabla_{\boldsymbol{\theta}} \nabla_{\boldsymbol{\theta}} h$.

To obtain the Hessian of \mathcal{L}_1 , we first introduce the Lagrangian:

$$\hat{\mathcal{L}}_1 = \sum_{m=0}^{N_t-1} \left(\mathbb{L}(t_m, \tilde{u}_1^m(\boldsymbol{\theta}), \tilde{u}_2^m(\boldsymbol{\theta})) + \varphi_1^{m\top} U_{1\text{FD}} + \varphi_2^{m\top} U_{2\text{FD}} \right). \quad (52)$$

Since by (50), $U_{1\text{FD}} = \mathbf{0}$ and $U_{2\text{FD}} = \mathbf{0}$, we may choose the Lagrange multipliers φ_1^m and φ_2^m freely. Consequently, we have $\hat{\mathcal{L}}_1 = \mathcal{L}_1$, and hence $\nabla_{\boldsymbol{\theta}} \hat{\mathcal{L}}_1 = \nabla_{\boldsymbol{\theta}} \mathcal{L}_1$, and $\nabla_{\boldsymbol{\theta}} \nabla_{\boldsymbol{\theta}} \hat{\mathcal{L}}_1 = \nabla_{\boldsymbol{\theta}} \nabla_{\boldsymbol{\theta}} \mathcal{L}_1$. In order to avoid long expressions, we set $\tilde{u}_{k\boldsymbol{\theta}}^m := \nabla_{\boldsymbol{\theta}} \tilde{u}_k^m$ and $\tilde{f}_{k\boldsymbol{\theta}}^m := \nabla_{\boldsymbol{\theta}} \tilde{f}_k^m$, with $k = 1, 2$. Thanks to (50), we have

$$\begin{aligned} \nabla_{\boldsymbol{\theta}} \hat{\mathcal{L}}_1 = & \sum_{m=0}^{N_t-1} \left(\nabla_{\tilde{u}_1^m} \mathbb{L} \tilde{u}_{1\boldsymbol{\theta}}^m + \nabla_{\tilde{u}_2^m} \mathbb{L} \tilde{u}_{2\boldsymbol{\theta}}^m + \varphi_1^{m\top} \left(I_1 \frac{\tilde{u}_{1\boldsymbol{\theta}}^{m+1} - 2\tilde{u}_{1\boldsymbol{\theta}}^m + \tilde{u}_{1\boldsymbol{\theta}}^{m-1}}{\Delta t^2} + \right. \right. \\ & I_2 \frac{\tilde{u}_{1\boldsymbol{\theta}}^{m+1} - \tilde{u}_{1\boldsymbol{\theta}}^{m-1}}{2\Delta t} - A_1 \tilde{u}_{1\boldsymbol{\theta}}^m - A_2 \tilde{u}_{2\boldsymbol{\theta}}^m - C \tilde{f}_{1\boldsymbol{\theta}}^m \Big) + \varphi_2^{m\top} \left(I_1 \frac{\tilde{u}_{2\boldsymbol{\theta}}^{m+1} - 2\tilde{u}_{2\boldsymbol{\theta}}^m + \tilde{u}_{2\boldsymbol{\theta}}^{m-1}}{\Delta t^2} \right. \\ & \left. \left. + I_2 \frac{\tilde{u}_{2\boldsymbol{\theta}}^{m+1} - \tilde{u}_{2\boldsymbol{\theta}}^{m-1}}{2\Delta t} - B_1 \tilde{u}_{1\boldsymbol{\theta}}^m - B_2 \tilde{u}_{2\boldsymbol{\theta}}^m - C \tilde{f}_{2\boldsymbol{\theta}}^m \right) \right). \end{aligned}$$

Using *summation by parts*, it is easy to show that the following relations hold for $k = 1, 2$,

$$\sum_{m=0}^{N_t-1} \varphi_k^{m\top} I_1 \frac{\tilde{u}_k^{m+1} - 2\tilde{u}_k^m + \tilde{u}_k^{m-1}}{\Delta t^2} = \sum_{m=0}^{N_t-1} \frac{\varphi_k^{m+1\top} - 2\varphi_k^{m\top} + \varphi_k^{m-1\top}}{\Delta t^2} I_1 \tilde{u}_k^m,$$

and

$$\sum_{m=0}^{N_t-1} \varphi_k^{m\top} I_2 \frac{\tilde{u}_k^{m+1} - \tilde{u}_k^{m-1}}{2\Delta t} = - \sum_{m=0}^{N_t-1} \frac{\varphi_k^{m+1\top} - \varphi_k^{m-1\top}}{2\Delta t} I_2 \tilde{u}_k^m.$$

Therefore,

$$\begin{aligned} \nabla_{\boldsymbol{\theta}} \hat{\mathcal{L}}_1 = & \sum_{m=0}^{N_t-1} \left((\nabla_{\tilde{u}_1^m} \mathbb{L} + \frac{\varphi_1^{m+1\top} - 2\varphi_1^{m\top} + \varphi_1^{m-1\top}}{\Delta t^2} I_1 - \frac{\varphi_1^{m+1\top} - \varphi_1^{m-1\top}}{2\Delta t} I_2 \right. \\ & - \varphi_1^{m\top} A_1 - \varphi_2^{m\top} B_1) \tilde{u}_1^m + (\nabla_{\tilde{u}_2^m} \mathbb{L} + \frac{\varphi_2^{m+1\top} - 2\varphi_2^{m\top} + \varphi_2^{m-1\top}}{\Delta t^2} I_1 \\ & \left. - \frac{\varphi_2^{m+1\top} - \varphi_2^{m-1\top}}{2\Delta t} I_2 - \varphi_1^{m\top} A_2 - \varphi_2^{m\top} B_2) \tilde{u}_2^m - \varphi_1^{m\top} C \tilde{f}_{1\boldsymbol{\theta}}^m - \varphi_2^{m\top} C \tilde{f}_{2\boldsymbol{\theta}}^m \right). \end{aligned}$$

Hence, if we let φ_1^m and φ_2^m be the solutions to the following dual problems,

$$\begin{aligned} \Phi_{1\text{FD}} \equiv & \frac{\varphi_1^{m+1\top} - 2\varphi_1^{m\top} + \varphi_1^{m-1\top}}{\Delta t^2} I_1 - \frac{\varphi_1^{m+1\top} - \varphi_1^{m-1\top}}{2\Delta t} I_2 \\ & - \varphi_1^{m\top} A_1 - \varphi_2^{m\top} B_1 + \nabla_{\tilde{u}_1^m} \mathbb{L} = 0, \end{aligned} \quad (53a)$$

$$\begin{aligned} \Phi_{2\text{FD}} \equiv & \frac{\varphi_2^{m+1\top} - 2\varphi_2^{m\top} + \varphi_2^{m-1\top}}{\Delta t^2} I_1 - \frac{\varphi_2^{m+1\top} - \varphi_2^{m-1\top}}{2\Delta t} I_2 \\ & - \varphi_1^{m\top} A_2 - \varphi_2^{m\top} B_2 + \nabla_{\tilde{u}_2^m} \mathbb{L} = 0, \end{aligned} \quad (53b)$$

then

$$\nabla_{\boldsymbol{\theta}} \hat{\mathcal{L}}_1 = - \sum_{m=0}^{N_t-1} \left(\varphi_1^{m\top} C \tilde{f}_{1\boldsymbol{\theta}}^m + \varphi_2^{m\top} C \tilde{f}_{2\boldsymbol{\theta}}^m \right).$$

In a similar way, we can differentiate twice the Lagrangian with respect to $\boldsymbol{\theta}$ and use (50) and (53) and summation by parts formulas to obtain

$$\nabla_{\boldsymbol{\theta}} \nabla_{\boldsymbol{\theta}} \hat{\mathcal{L}}_1 = H_I + H_{II},$$

where

$$H_I = \sum_{m=0}^{N_t-1} \left((\tilde{u}_{1\boldsymbol{\theta}}^m)^\top (\nabla_{\tilde{u}_1^m} \nabla_{\tilde{u}_1^m} \mathbb{L})(\tilde{u}_{1\boldsymbol{\theta}}^m) + (\tilde{u}_{2\boldsymbol{\theta}}^m)^\top (\nabla_{\tilde{u}_2^m} \nabla_{\tilde{u}_2^m} \mathbb{L})(\tilde{u}_{2\boldsymbol{\theta}}^m) \right), \quad (54)$$

$$H_{II} = - \sum_{m=0}^{N_t-1} \sum_{i=1}^{N_h} \left((\varphi_1^{m\top} C)_i \nabla_{\boldsymbol{\theta}} \tilde{f}_{1\boldsymbol{\theta}}^m(i, :) + (\varphi_2^{m\top} C)_i \nabla_{\boldsymbol{\theta}} \tilde{f}_{2\boldsymbol{\theta}}^m(i, :) \right). \quad (55)$$

Here, $(y)_i \in \mathbb{R}$ means the i -th entry of a vector, $y \in \mathbb{R}^{1 \times N_h}$, and $\tilde{f}_\theta(i, :) \in \mathbb{R}^{1 \times N_\theta}$ means the i -th row of a matrix, $\tilde{f}_\theta \in \mathbb{R}^{N_h \times N_\theta}$. Note that, in this case, we will have $\nabla_\theta \tilde{f}_\theta(i, :) \in \mathbb{R}^{N_\theta \times N_\theta}$.

We finally obtain the Hessian of the cost functional,

$$\nabla_\theta \nabla_\theta \mathcal{L} = H_I + H_{II} - \nabla_\theta \nabla_\theta h, \quad (56)$$

where H_I and H_{II} are given by (54)-(55). The computation of the second term of the Hessian, H_{II} , requires solving one dual problem (53) and one full elastic wave equation (50) to obtain \tilde{u}_k^m and consequently $\nabla_{\tilde{u}_k^m} \mathbb{L}$, with $k = 1, 2$. However, calculating the first term, H_I , requires the quantities $\tilde{u}_{1\theta}^m$ and $\tilde{u}_{2\theta}^m$, which satisfy the elastic wave equation with the force term \mathbf{f}_θ . Therefore, in total, $N_\theta + 2$ wave equations must be solved to compute the Hessian (56).

Remark 2. We note that in practice, we only compute the first part of the Hessian H_I (see Theorem 4) for which we need to solve N_θ primal problems. If higher accuracy and consequently the computation of the second part of the Hessian H_{II} is needed (see Theorem 3), we also need to solve one primal and one dual problem (53).

In order to further clarify the calculation of the Hessian, we address the following two issues:

1. Calculation of $\nabla_{\tilde{u}_k^m} \mathbb{L}$ and $\nabla_{\tilde{u}_k^m} \nabla_{\tilde{u}_k^m} \mathbb{L}$, with $k = 1, 2$. By the definition of \mathbb{L} in (51), we have

$$\nabla_{\tilde{u}_k^m} \mathbb{L} = \sum_{r=1}^{N_R} \mathbf{r}_r(t_m, \theta)^\top \mathbf{C}_\epsilon^{-1} \nabla_{\tilde{u}_k^m} \mathbf{r}_r(t_m, \theta),$$

Note that by (8) and (10), we have

$$\nabla_{\tilde{u}_1^m} \mathbf{r}_r = \begin{pmatrix} 0 & \dots & 0 & -1 & 0 & \dots & 0 \\ 0 & & & \dots & & & 0 \end{pmatrix}, \quad \nabla_{\tilde{u}_2^m} \mathbf{r}_r = \begin{pmatrix} 0 & & & \dots & & & 0 \\ 0 & \dots & 0 & -1 & 0 & \dots & 0 \end{pmatrix},$$

which are $2 \times N_h$ matrices with zero elements except one element being -1 corresponding to the receiver, r . Similarly, we obtain $\nabla_{\tilde{u}_k^m} \nabla_{\tilde{u}_k^m} \mathbb{L} \in \mathbb{R}^{N_h \times N_h}$ with zero elements except for N_R diagonal elements being \hat{c}_{11} at the locations corresponding to N_R receivers. We note that for computing $\nabla_{\tilde{u}_k^m} \mathbb{L}$, we need \tilde{u}_k^m , but $\nabla_{\tilde{u}_k^m} \nabla_{\tilde{u}_k^m} \mathbb{L}$ is independent of \tilde{u}_k^m .

2. Discretization of the singular source function. We need to discretize the source function, \mathbf{f} , in (3) so that it is twice continuously differentiable with respect to θ (see (55)). In other words, the gradient of the Dirac distribution, $\nabla \delta(\mathbf{x} - \mathbf{x}_s)$, needs to be discretized so that it is twice continuously differentiable in \mathbf{x}_s . For this purpose, we employ the technique proposed in [21] to derive regularized approximations of the Dirac distribution and its gradient, which result in point-wise convergence of the solution away from the sources. The derivation of approximations of the Dirac distribution and its gradient is based on the following properties:

$$\int \phi(\mathbf{x}) \delta(\mathbf{x} - \mathbf{x}_s) d\mathbf{x} = \phi(\mathbf{x}_s), \quad \int \phi(\mathbf{x}) \partial_x \delta(\mathbf{x} - \mathbf{x}_s) d\mathbf{x} = -\partial_x \phi(\mathbf{x}_s),$$

which hold for any smooth, compactly supported function, ϕ . In one dimension with a uniform grid, x_k , with grid size h , the integrals are replaced by a discrete scalar product, $(p, q)_{1,h} := h \sum p_i q_i$. Fourth-order accurate approximations of the Dirac distribution and its gradient are for instance obtained when the integral conditions are satisfied with ϕ being polynomials of degree four. Let $x_k \leq x_s < x_{k+1}$ and $\alpha = (x_s - x_k)/h$. Then a fourth-order discretization of $\delta(x - x_s)$, which is twice continuously differentiable in \mathbf{x}_s , is given by [21]:

$$\begin{aligned}\delta_{k-2} &= (\alpha/12 - \alpha^2/24 - \alpha^3/12 - 19\alpha^4/24 + P(\alpha))/h, \\ \delta_{k-1} &= (-2\alpha/3 + 2\alpha^2/3 + \alpha^3/6 + 4\alpha^4 - 5P(\alpha))/h, \\ \delta_k &= (1 - 5\alpha^2/4 - 97\alpha^4/12 + 10P(\alpha))/h, \\ \delta_{k+1} &= (2\alpha/3 + 2\alpha^2/3 - \alpha^3/6 + 49\alpha^4/6 - 10P(\alpha))/h, \\ \delta_{k+2} &= (-\alpha/12 - \alpha^2/24 + \alpha^3/12 - 33\alpha^4/8 + 5P(\alpha))/h, \\ \delta_{k+3} &= (5\alpha^4/6 - P(\alpha))/h, \\ \delta_j &= 0, \quad j \notin \{k-1, k, k+1, k+2\},\end{aligned}$$

where $P(\alpha) = 5\alpha^5/3 - 7\alpha^6/24 - 17\alpha^7/12 + 9\alpha^8/8 - \alpha^9/4$. Similarly, a fourth-order discretization of $\delta'(x - x_s)$ is given by

$$\begin{aligned}\delta'_{k-2} &= (-1/12 + \alpha/12 + \alpha^2/4 + 2\alpha^3/3 + R(\alpha))/h^2, \\ \delta'_{k-1} &= (2/3 - 4\alpha/3 - \alpha^2/2 - 7\alpha^3/2 - 5R(\alpha))/h^2, \\ \delta'_k &= (5\alpha/2 + 22\alpha^3/3 + 10R(\alpha))/h^2, \\ \delta'_{k+1} &= (-2/3 - 4\alpha/3 + \alpha^2/2 - 23\alpha^3/3 - 10R(\alpha))/h^2, \\ \delta'_{k+2} &= (1/12 + \alpha/12 - \alpha^2/4 + 4\alpha^3 + 5R(\alpha))/h^2, \\ \delta'_{k+3} &= (-5\alpha^3/6 - R(\alpha))/h^2, \\ \delta'_j &= 0, \quad j \notin \{k-1, k, k+1, k+2\},\end{aligned}$$

where $R(\alpha) = -25\alpha^4/12 - 3\alpha^5/4 + 59\alpha^6/12 - 4\alpha^7 + \alpha^8$. A two-dimensional approximation can for instance be obtained by Cartesian products of one-dimensional discretizations:

$$\delta(\mathbf{x} - \mathbf{x}_s) \approx \delta(x_1 - x_{1s}) \delta(x_2 - x_{2s}), \quad \nabla \delta(\mathbf{x} - \mathbf{x}_s) \approx \begin{pmatrix} \delta'(x_1 - x_{1s}) \delta(x_2 - x_{2s}) \\ \delta(x_1 - x_{1s}) \delta'(x_2 - x_{2s}) \end{pmatrix}.$$

This representation of the forcing together with the second-order accurate finite difference scheme, presented in Section 3.3.1, result in an overall second-order convergence of the solution away from the singularity at \mathbf{x}_s (see also [14]).

The complete algorithm for computing the Hessian is outlined in Algorithm 1.

3.3.3. The scaled Hessian

In seismic source inversion, the parameters span several magnitudes. For example, the time shift and frequency are $\mathcal{O}(1)$ and the source momenta are $\mathcal{O}(10^{14})$, which potentially lead to a Hessian matrix with a large condition number. To deal with this problem, we carry out a change of variables as follows:

$$\tilde{\boldsymbol{\theta}} = \mathbf{S}\boldsymbol{\theta} \quad \text{with} \quad \mathbf{S} = \sqrt{\text{diag}(\mathbf{H}_1)}.$$

Algorithm 1 Calculate the Hessian of the cost functional given a $\boldsymbol{\theta}^*$

Calculate H_I :

1. Discretize the source function \mathbf{f} and obtain $\tilde{f}_k(t; \boldsymbol{\theta}^*)$ for $k = 1, 2$.
2. Calculate $\partial_{\theta_j} \tilde{f}_k(t; \boldsymbol{\theta}^*)$ for $j = 1, \dots, N_\theta$ by differentiating $\tilde{f}_k(t; \boldsymbol{\theta}^*)$ in step 1.
3. Solve (50) with forces in step 2 and obtain \tilde{u}_k^m for $k = 1, 2$.
4. Find $\nabla_{\tilde{u}_k^m} \nabla_{\tilde{u}_k^m} \mathbb{L}$ for $k = 1, 2$.
5. Compute H_I by (54).

Calculate H_{II} :

6. Solve (50) with forces in step 1 and obtain \tilde{u}_k^m for $k = 1, 2$.
 7. Find $\nabla_{\tilde{u}_k^m} \mathbb{L}$ for $k = 1, 2$.
 8. Solve (53) and obtain φ_k^m for $k = 1, 2$.
 9. Calculate $\nabla_{\boldsymbol{\theta}} \tilde{f}_k^m$ by differentiating $\partial_{\theta_j} \tilde{f}_k(t; \boldsymbol{\theta}^*)$ in step 2.
 10. Compute H_{II} by (55).
-

Consequently, the rescaled Hessian reads:

$$\tilde{\mathbf{H}} = \mathbf{S}^{-\top} \mathbf{H}_1 \mathbf{S}^{-1},$$

and the information gain in the new scaled variables is:

$$\begin{aligned} D_{KL} &= \int_{\tilde{\boldsymbol{\Theta}}} \log \left(\frac{p_{\tilde{\boldsymbol{\Theta}}}(\tilde{\boldsymbol{\theta}}|\{\mathbf{y}_r\})}{p_{\tilde{\boldsymbol{\Theta}}}(\tilde{\boldsymbol{\theta}})} \right) p_{\tilde{\boldsymbol{\Theta}}}(\tilde{\boldsymbol{\theta}}|\{\mathbf{y}_r\}) d\tilde{\boldsymbol{\theta}} \\ &= -\frac{1}{2} \log((2\pi)^{N_\theta} |\tilde{\mathbf{H}}(\hat{\boldsymbol{\theta}})^{-1}|) - \frac{N_\theta}{2} + \tilde{h}(\hat{\boldsymbol{\theta}}) + \frac{\tilde{\mathbf{H}}(\hat{\boldsymbol{\theta}})^{-1} : \nabla_{\tilde{\boldsymbol{\theta}}} \nabla_{\tilde{\boldsymbol{\theta}}} \tilde{h}(\hat{\boldsymbol{\theta}})}{2} + \mathcal{O}_P(\mathbf{S}(\hat{\boldsymbol{\theta}} - \boldsymbol{\theta}^*)), \end{aligned} \quad (57)$$

where $p_{\tilde{\boldsymbol{\Theta}}}(\tilde{\boldsymbol{\theta}}|\{\mathbf{y}_r\}) = p_{\boldsymbol{\Theta}}(\mathbf{S}^{-1}\tilde{\boldsymbol{\theta}}|\{\mathbf{y}_r\})|\mathbf{S}|^{-1}$, $p_{\tilde{\boldsymbol{\Theta}}}(\tilde{\boldsymbol{\theta}}) = p_{\boldsymbol{\Theta}}(\mathbf{S}^{-1}\tilde{\boldsymbol{\theta}})|\mathbf{S}|^{-1}$, and $\tilde{h}(\boldsymbol{\theta}) = \log p_{\tilde{\boldsymbol{\Theta}}}(\boldsymbol{\theta})$. We approximate $\hat{\boldsymbol{\theta}}$ by $\boldsymbol{\theta}^*$, such that Theorem 4 can be applied to compute the expected information gain.

3.3.4. Numerical integration

In this section, we briefly review two approaches for numerical integration, namely the deterministic sparse quadrature and Monte Carlo random sampling. Note that we use the sparse quadrature under the assumption that the corresponding integrand has a certain level of regularity. We should resort to sampling based numerical integration techniques, e.g., Monte Carlo sampling, when this assumption is not valid. Due to the singular source term and its twice continuously differentiable discretization, the solution of our problem does not possess high regularity with respect to the source location parameters.

For details of sparse quadratures, see [1, 2, 3, 17, 22]. Also, see [14, 15] for a detailed regularity analysis and convergence study of the sparse quadrature for the stochastic wave

equation. We can use the interpolating polynomial-based numerical integration and write

$$I = \int_{\Theta} \hat{D}_{KL}(\boldsymbol{\theta}^*) p(\boldsymbol{\theta}^*) d\boldsymbol{\theta}^* = \sum_{i=1}^{\eta} w_i \hat{D}_{KL}(\boldsymbol{\theta}_i^*) + \varepsilon_{\eta}, \quad (58)$$

where $\{\boldsymbol{\theta}_i^*\}_{i=1}^{\eta}$ and $\{w_i\}_{i=1}^{\eta}$ are η quadrature points and weights, respectively, \hat{D}_{KL} is the approximated K–L divergence given by (24), and ε_{η} is the interpolation error. Different types of quadrature rules are available, including Gauss and Clenshaw-Curtis rules. In Gauss quadrature, quadrature points and weights correspond to the multivariate p -orthogonal polynomials. For instance, Legendre and Hermite polynomials are used for uniform and Gaussian priors, respectively. In Clenshaw-Curtis quadrature, Chebyshev polynomials are employed to obtain quadrature points and weights.

In a standard quadrature rule on full tensor product grids, the total number of quadrature points, η , grows exponentially with N_{θ} . Full tensor product approximations can therefore be used only when the number of parameters is small (in practice when $N_{\theta} \leq 3$). In order to suppress the curse of dimensionality, sparse quadrature rules are employed. The main strategy used in sparse quadrature is to leave out the fine levels of a hierarchical interpolation. A full tensor product rule is recovered if all the hierarchical bases are used. Sparse approximations are both accurate and efficient, particularly when the integrand, $\hat{D}_{KL}(\boldsymbol{\theta}^*)$, is highly regular with respect to $\boldsymbol{\theta}^*$. In general, the following estimates hold for full tensor quadrature rules:

$$\hat{D}_{KL} \in H^s(\mathbb{R}^{N_{\theta}}) \quad \Rightarrow \quad \varepsilon_{\eta} = \mathcal{O}(\eta^{-s/N_{\theta}}),$$

and for sparse quadrature rules:

$$\hat{D}_{KL} \in H_{\text{mix}}^s(\mathbb{R}^{N_{\theta}}) \quad \Rightarrow \quad \varepsilon_{\eta} = \mathcal{O}(\eta^{-s}(\log \eta)^{s(N_{\theta}-1)}).$$

Here, H^s is the space of multi-variate functions with square integrable $s > 0$ weak derivatives with respect to each variable, and H_{mix}^s is the space of multi-variate functions with square integrable $s > 0$ *mixed* weak derivatives. See [18, 15, 14] for more details.

On the other hand, if we use Monte Carlo random sampling, the expected information gain can be written as

$$I = \int_{\Theta} \hat{D}_{KL}(\boldsymbol{\theta}^*) p(\boldsymbol{\theta}^*) d\boldsymbol{\theta}^* = \frac{1}{M} \sum_{j=1}^M \hat{D}_{KL}(\boldsymbol{\theta}_j^*) + \varepsilon_M, \quad (59)$$

where $\boldsymbol{\theta}_j^*$ is the j^{th} random sample drawn from distribution $p(\boldsymbol{\theta}^*)$, and $\varepsilon_M = \mathcal{O}_P(M^{-1/2})$.

We note that recent advances in Monte Carlo type methods, such as multilevel Monte Carlo [7] and multi-index Monte Carlo [9], can be used to accelerate the computation of expected information gain, when the dimension is high and/or the integrand function lacks high regularity with respect to the parameters.

Remark 3. In addition to the quadrature error, ε_η or ε_M , we also need to consider the discretization error in the computation of Hessian, which is proportional to h^q , where q depends on the order of accuracy of the finite difference scheme and the regularity of the wave solution. In practice, we take the spatial grid-length h small enough so that the discretization error does not dominate the quadrature error.

4. Numerical Examples

In this section, we present a few numerical examples to demonstrate the efficiency and applicability of the numerical method for the fast estimation of the expected information gain described above.

4.1. Model problem

We consider a layered isotropic elastic material in a two-dimensional space and model a simplified earthquake, which is similar to the layer over half space problem called LOH.1 [6]. The top layer, D_I , extends over $-1000 \leq x_2 \leq 0$, and the half space, D_{II} , is given by $x_2 \leq -1000$. We truncate the domain and consider the box $D = [-10000, 10000] \times [-15000, 0]$. We impose the stress-free boundary condition on the free surface, $x_2 = 0$, and the first-order Clayton-Engquist non-reflecting boundary conditions [5] at the artificial boundaries. The material density and velocities are given by

$$\nu(\mathbf{x}) = \begin{cases} 2600 & \mathbf{x} \in D_I \\ 2700 & \mathbf{x} \in D_{II} \end{cases} \quad c_p(\mathbf{x}) = \begin{cases} 4000 & \mathbf{x} \in D_I \\ 6000 & \mathbf{x} \in D_{II} \end{cases} \quad c_s(\mathbf{x}) = \begin{cases} 2000 & \mathbf{x} \in D_I \\ 3464 & \mathbf{x} \in D_{II} \end{cases}$$

A point moment tensor forcing is applied with a Gaussian time function,

$$S(t; t_s, \omega_s) = \frac{\omega_s}{\sqrt{2\pi}} e^{-\omega_s^2 (t-t_s)^2/2},$$

which is parametrized by the frequency ω_s and the center time t_s . Except for the convergence study in Section 4.3, for all experiments, we consider uniform priors for all $N_\theta = 7$ parameters:

$$\theta_1 \sim \mathcal{U}(-1000, 1000), \quad \theta_2 \sim \mathcal{U}(-3000, -1000), \quad \theta_3 \sim \mathcal{U}(0.5, 1.5),$$

$$\theta_4 \sim \mathcal{U}(3, 5), \quad \theta_5, \theta_6, \theta_7 \sim \mathcal{U}(10^{13}, 10^{15}).$$

Here, the vector of parameters reads $\boldsymbol{\theta} = (x_{1s}, x_{2s}, t_s, \omega_s, m_{x_1x_1}, m_{x_1x_2}, m_{x_2x_2})^\top$.

The array of receivers is placed on the ground surface. See Figure 1. The observation vector contains all displacements measured at the receivers. We assume that the measurement errors for the horizontal and vertical displacements at each receiver are independent Gaussian random variables, $\boldsymbol{\epsilon}_r \sim \mathcal{N}(\mathbf{0}, \mathbf{C}_\epsilon)$, with $\mathbf{C}_\epsilon = \begin{pmatrix} 0.0001 & 0 \\ 0 & 0.0001 \end{pmatrix}$ for all receivers, $r = 1, \dots, N_R$. We employ the second-order finite difference approximation proposed in [16] with a fixed spatial grid-length, $h = 200$, and a time step, $\Delta t = 0.025$. The elastic wave

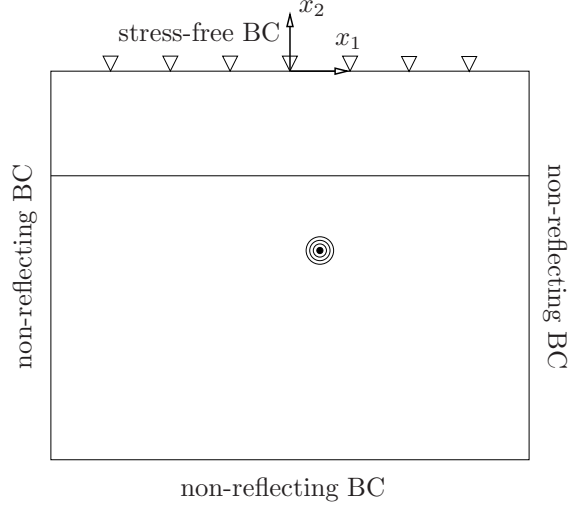


Figure 1: The two-layered spatial domain $D = [-10000, 10000] \times [-15000, 0]$ with stress-free and non-reflecting boundary conditions. An array of N_R receivers are located on the ground surface in equidistant recording points.

equation is integrated to the time, $T = 8$. We note that $h = 200$ is the largest spatial grid-length for which the discretization error, which is proportional to $\mathcal{O}(h^2)$, does not dominate the quadrature error in the integration of the information gain (59) with respect to the prior distribution. We record the wave solutions at $N_t = 1 + T/\Delta t = 321$ discrete time levels. For example, Figure 2 shows the ground motions at the receiver station, $\mathbf{x}_0 = (5000, 0)$, as a function of time, due to solving the elastic wave equation with the prior source parameters, $\mathbb{E}[\boldsymbol{\theta}] = (0, -2000, 1, 4, 10^{14}, 10^{14}, 10^{14})^\top$.

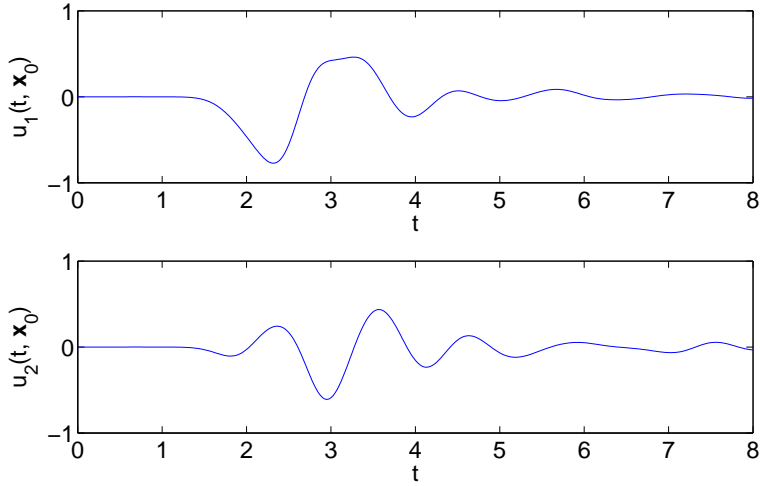


Figure 2: The ground motions versus time at the receiver station, $\mathbf{x}_0 = (5000, 0)$. The motions are due to solving the elastic wave equation with the prior source parameters, $\mathbb{E}[\boldsymbol{\theta}] = (0, -2000, 1, 4, 10^{14}, 10^{14}, 10^{14})^\top$.

4.2. The scaled Hessian

The sizes of the source parameters span many orders of magnitude. In SI units, we have

$$\theta_1, \theta_2 = \mathcal{O}(10^4) \text{ m}, \quad \theta_3 = \mathcal{O}(1) \text{ s}, \quad \theta_4 = \mathcal{O}(10) \text{ 1/s}, \quad \theta_5, \theta_6, \theta_7 = \mathcal{O}(10^{13}) - \mathcal{O}(10^{15}) \text{ Ns}.$$

Consequently, the condition number of the Hessian is very large. The Hessian therefore is scaled, as described in Section 3.3.3. For more clarification, we compute the Hessian matrix, \mathbf{H}_1 , in (54) for the expected value of the prior source parameters, $\mathbb{E}[\boldsymbol{\theta}] = (0, -2000, 1, 4, 10^{14}, 10^{14}, 10^{14})^\top$. The condition number of the unscaled Hessian computed by MATLAB is $\text{cond}(\mathbf{H}_1) = 3.88 \times 10^{30}$. Now, if we use the scaling matrix, $\mathbf{S} \in \mathbb{R}^{7 \times 7}$, with diagonal elements, $S_{ii} = \sqrt{H_{1ii}}$, and zero off-diagonal elements, then the condition number of the scaled Hessian, $\hat{\mathbf{H}}_1 = \mathbf{S}^{-\top} \mathbf{H}_1 \mathbf{S}^{-1}$, reduces significantly to $\text{cond}(\hat{\mathbf{H}}_1) = 12.16$.

4.3. Convergence of sparse quadrature

In this section, we numerically study the convergence of the two quadrature techniques based on sparse grids and Monte Carlo samples. We consider three parameters:

$$\theta_2 \sim \mathcal{U}(-3000, -1000), \quad \theta_4 \sim \mathcal{U}(3, 5), \quad \theta_5 \sim \mathcal{U}(10^{13}, 10^{15})$$

and leave the other four parameters fixed, i.e. $\theta_1 = -1000, \theta_3 = 1$, and $\theta_6 = \theta_7 = 10^{14}$. We use a Gauss-Legendre sparse grid based on a total degree multi-index set. See [12] for details on the construction of sparse grids. We consider a sequence of twenty sparse grids with $\eta_i = 351, 681, \dots, 271857$ quadrature points. The sparse grids correspond to three directions and are obtained by total degree index sets. We then compute the relative error,

$$\varepsilon_{\eta_i} = \frac{|I_{\eta_{i+1}} - I_{\eta_i}|}{|I_{\eta_{i+1}}|}, \quad i = 1, \dots, 19.$$

We also consider a sequence of $M_i = 10^2, 10^3, 10^4, 5 \times 10^4, 10^5$ random samples and carry on ten realizations of each M_i . In a similar way as above, we compute the relative error ε_{M_i} in the Monte Carlo sampling technique. Figure 3 shows the relative errors in sparse quadrature ε_η and in Monte Carlo sampling technique ε_M , versus the number of quadrature points η and the number of samples M . A simple linear regression through the data points shows that the rate of convergence of sparse quadrature is 0.40, while the rate of convergence of Monte Carlo is 0.49. The slow rate of convergence in sparse quadrature is a result of low regularity of I with respect to $\boldsymbol{\theta}$. Specifically, the solution of our problem does not have high regularity with respect to the parameters of source location, due to the singular source term. However, the regularity needed to satisfy Assumptions 1 and 2 can still be provided by the twice continuously differentiable discretization of the delta function in the source term.

4.4. Comparison of Laplace method and nested Monte Carlo Sampling

We numerically verify the concentration of measure by comparing the results of Laplace method (sparse quadrature) and direct nested Monte Carlo sampling. We assume three parameters are known with values identical to those in the previous subsection. We collect

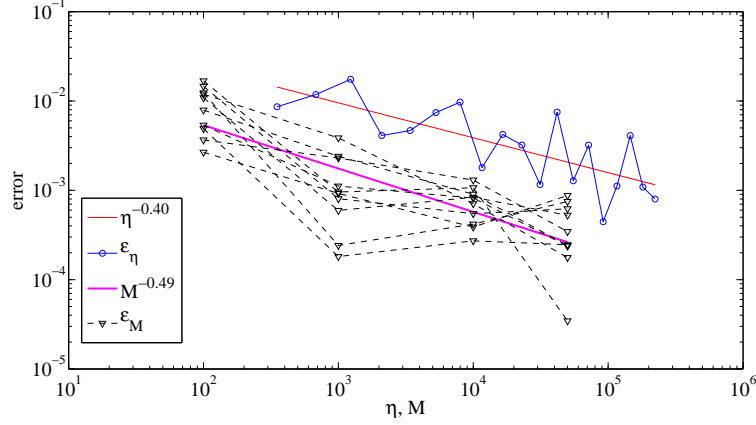


Figure 3: The relative errors in sparse quadrature and Monte Carlo versus the number of quadrature points and samples. The rate of convergence, obtained by linear regression through the data points, is 0.40 for sparse quadrature and 0.49 for Monte Carlo sampling.

data for a period of $T = 1.25$ at two receivers located at $x_1 = -9000$ and $x_1 = 1000$. The values of expected information gains computed by both methods with respect to the number of samples/quadratures are shown in Figure 4. Note that the Laplace method converges much faster than the nested Monte Carlo and the difference between the final results is less than 4%. The strong bias in the nested Monte Carlo is due to the fact that we reused the samples in the inner and outer loops.

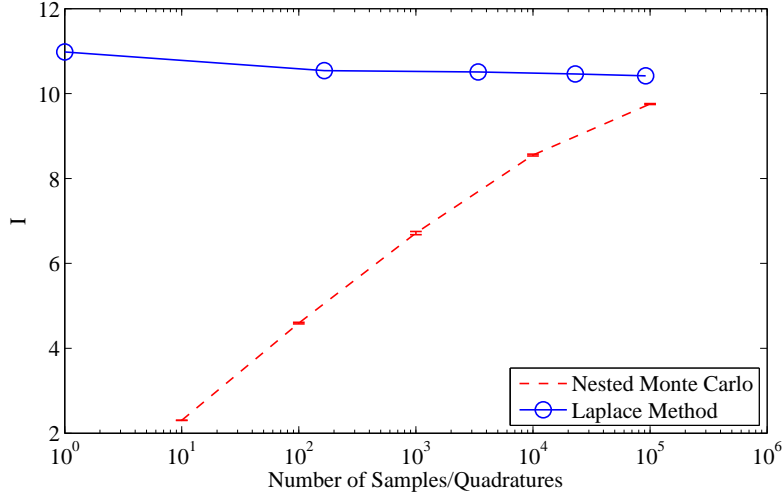


Figure 4: Comparison of the convergence performances of Laplace method and nested Monte Carlo sampling.

4.5. Experimental setups

We carry out three sets of experiments for the model problem in Section 4.1:

- **Scenario I:** The number of receivers and the distance between the receivers vary, but the interval on which the receivers are distributed evenly and symmetrically around $x_1 = 0$ is fixed, $[-8000, 8000]$. In particular, we consider the following settings:

N_R	3	5	9	17	41	81
d_R	8000	4000	2000	1000	400	200

giving a total of six experiments. d_R is the distance between two consecutive receivers.

- **Scenario II:** The number of receivers varies, $N_R = 1, 3, 5, \dots, 19$, and the distance between the receivers is fixed, $d_R = 1000$. We distribute the receivers evenly and symmetrically around $x_1 = 0$. This gives a total of 10 experiments.
- **Scenario III:** The number of receivers is fixed, $N_R = 5$, and the distance between the receivers varies, $d_R = 200, 400, 600, \dots, 4000$. We distribute the receivers evenly and symmetrically around $x_1 = 0$. This gives a total of 20 experiments.

Figure 5 shows the expected information gain, computed both by Monte Carlo sampling with $M = 10^4$ samples and by sparse quadrature with $\eta = 8583$ quadrature points, for six experiments in scenario I. The expected information gain increases sharply until the number of seismograms reaches 20. The extra gains of information is marginal when the number of seismograms is more than 20,

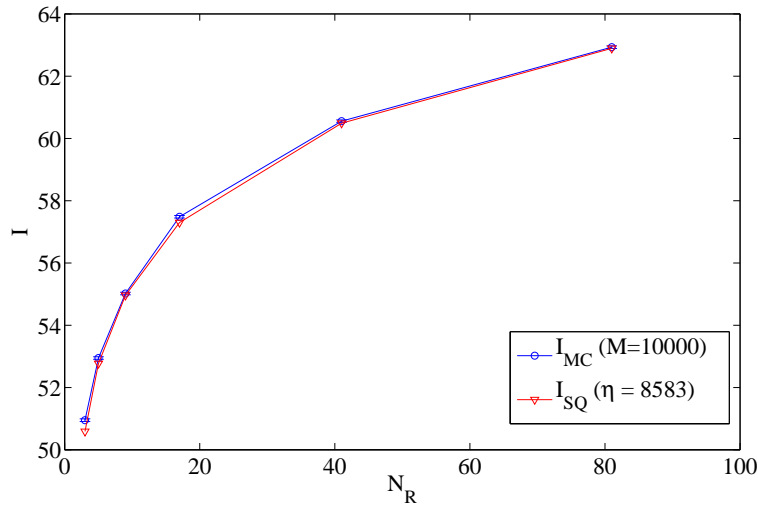


Figure 5: The expected information gain, computed both by Monte Carlo sampling with $M = 10^4$ samples (together with 68.27% confidence interval) and by sparse quadrature with $\eta = 8583$ quadrature points, for six experiments in scenario I. The confidence intervals are indeed very small, less than 1%.

Figure 6 shows the expected information gain, computed both by Monte Carlo sampling with $M = 10^4$ samples and by sparse quadrature with $\eta = 8583$ quadrature points, for 10

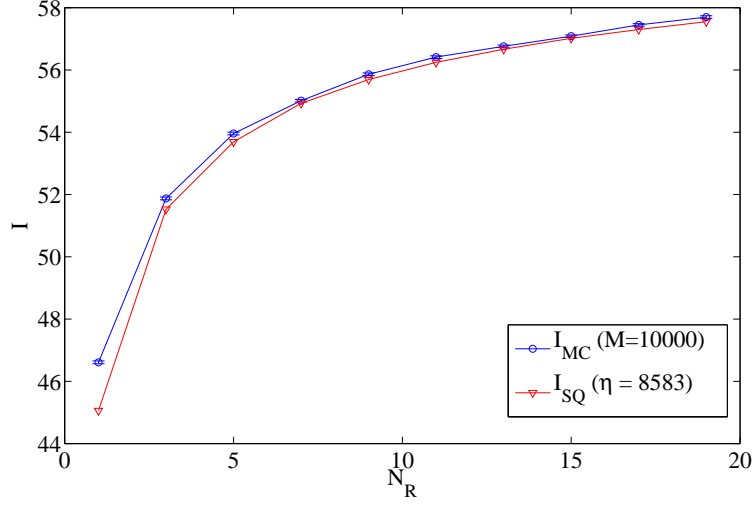


Figure 6: The expected information gain, computed both by Monte Carlo sampling with $M = 10^4$ samples (together with 68.27% confidence interval) and by sparse quadrature with $\eta = 8583$ quadrature points, for 10 experiments in scenario II.

experiments in scenario II. It shows that as we increase the number of seismograms, the information gain increases marginally.

Figure 7 shows the expected information gain, computed both by Monte Carlo sampling with $M = 10^4$ and $M = 10^5$ samples and by sparse quadrature with $\eta = 8583$ and $\eta = 26769$ quadrature points, for 20 experiments in scenario III. It shows that the experiment with $d_R = 1000$ gives the maximum information. Both lumping and sparsifying the seismograms give suboptimal designs.

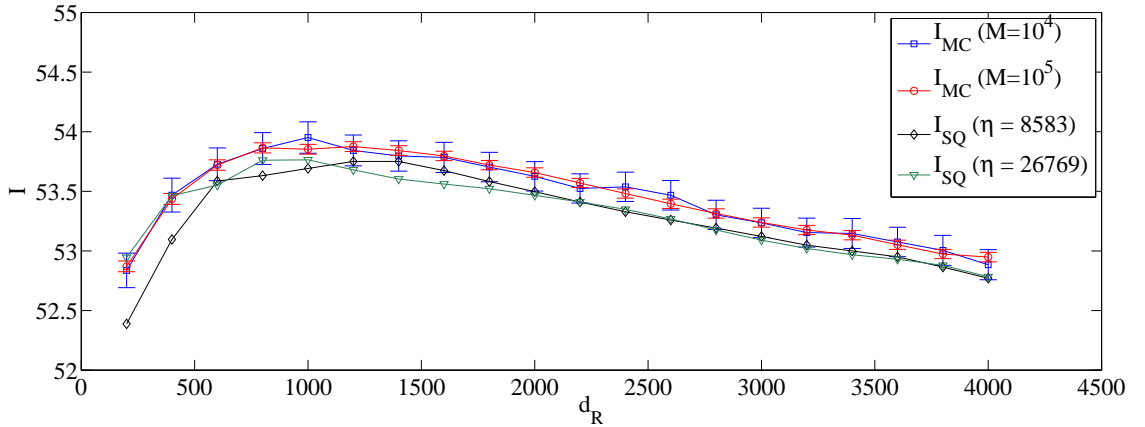


Figure 7: The expected information gain, computed both by Monte Carlo sampling (together with 99.7% confidence interval) and by sparse quadrature, for 20 experiments in scenario III.

Figure 8 shows seven quantities of interest, Q_{θ_i} with $i = 1, \dots, 7$, which represent the information gains of each parameter separately, computed by Monte Carlo sampling with $M = 10^5$ samples for 20 experiments in scenario III. The experiment with approximately $d_R = 1000$ gives the maximum information for θ_2 , θ_6 and θ_7 . The experiment with approximately $d_R = 500$ gives the maximum information for θ_4 . The experiment with approximately $d_R = 2000$ gives the maximum information for θ_5 . However, sparsifying the seismograms does not induce a drop of information gain in θ_1 and θ_3 .

Note that we simply sweep over the design spaces to search for the optimal designs because all the scenarios we considered are one-dimensional with respect to the experimental setup, ξ . In the cases that more freedom is allowed in a higher dimensional design space, more advanced optimisation algorithm should be implemented.

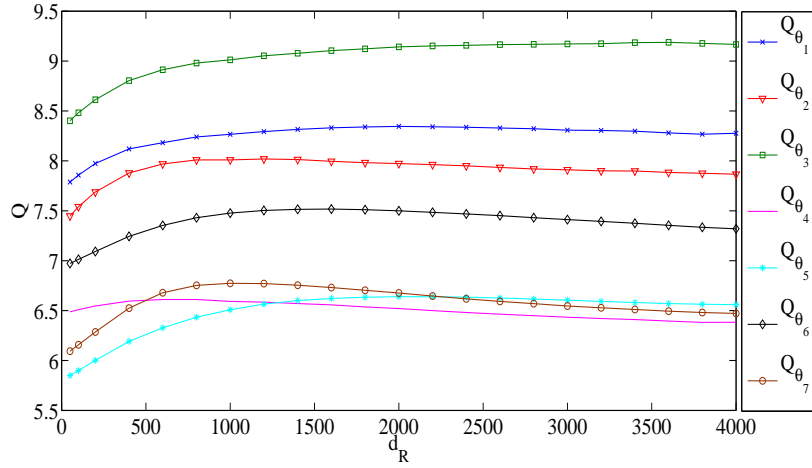


Figure 8: The expected information gain corresponding to each parameter separately, computed by Monte Carlo sampling with $M = 10^5$ samples for 20 experiments in scenario III.

5. Conclusion

We have developed a fast method of optimal experimental design for statistical seismic source inversion in a Bayesian setting. This method can be generally applied to the design of non-repeatable experiments with a time-dependent model, as long as the assumptions in Section 3 are fulfilled. Taking into account that the Hessian of the cost functional is proportional to the product of the number of points in the time series of the measurements and the number of receivers, we use Laplace approximation to derive an analytical form of the information gain, which is a function of the determinant of the aforementioned Hessian matrix. The expected information gain eventually reduces to a marginalization of the information gain over all possible values of the unknown source parameters. The asymptotic error terms have been derived. We have applied the new technique to the optimal design of the number and location of seismic receivers on the ground for a simplified two-dimensional earthquake.

Acknowledgements

The authors are thankful for support from the Academic Excellency Alliance UT Austin-KAUST project—Uncertainty quantification for predictive modeling of the dissolution of porous and fractured media. Quan Long and Raul Tempone are members of the KAUST SRI Center for Uncertainty Quantification in Computational Science and Engineering.

Appendix A.

In this appendix, we show that

$$\sum_{r=1}^{N_R} \sum_{m=0}^{N_t-1} \boldsymbol{\epsilon}_r^\top \mathbf{C}_\epsilon^{-\top} \nabla_{\boldsymbol{\theta}} \mathbf{g}_r(t_m, \boldsymbol{\theta}^*) = \mathcal{O}_P(N^{1/2}).$$

For simplicity and to avoid tensor notations, we consider only the one-dimensional case, i.e., $d = 1$. The case when $d \geq 2$ follows in a similar way and with no difficulty.

We first note that when $d = 1$, $\mathbf{g}_r(t_m, \boldsymbol{\theta}) = u(t_m, x_r; \boldsymbol{\theta})$, $\boldsymbol{\epsilon}_r = \epsilon_r$, and $\mathbf{C}_\epsilon = c_\epsilon$ are scalar quantities. Now, let $u(t_m, x; \boldsymbol{\theta})$ be discretized on a spatial grid with N_h grid points. We collect u on all grid points in a N_h -vector denoted by $\tilde{u}(t_m, \boldsymbol{\theta})$. By the chain rule, we have

$$\nabla_{\boldsymbol{\theta}} u(t_m, x_r; \boldsymbol{\theta}^*) = \nabla_{\tilde{u}} u(t_m, x_r; \boldsymbol{\theta}^*) \nabla_{\boldsymbol{\theta}} \tilde{u}(t_m, \boldsymbol{\theta}^*).$$

Moreover, since $\partial_{u(t_m, x; \boldsymbol{\theta})} u(t_m, x_r; \boldsymbol{\theta}) = \delta(x - x_r)$, then

$$\nabla_{\tilde{u}} u(t_m, x_r; \boldsymbol{\theta}) = [0, \dots, 0, 1, 0, \dots, 0] =: \mathbb{I}_r,$$

where \mathbb{I}_r denotes a $1 \times N_h$ vector whose elements are zero, except a 1 at the position of the r -th recorder in the grid, denoted by $j(r)$. Therefore,

$$\sum_{r=1}^{N_R} \sum_{m=0}^{N_t-1} \epsilon_r^\top \mathbf{C}_\epsilon^{-\top} \nabla_{\boldsymbol{\theta}} \mathbf{g}_r(t_m, \boldsymbol{\theta}^*) = \sum_{r=1}^{N_R} \frac{\epsilon_r}{c_\epsilon} \mathbb{I}_r \sum_{m=0}^{N_t-1} \nabla_{\boldsymbol{\theta}} \tilde{u}(t_m, \boldsymbol{\theta}^*).$$

Note that $\nabla_{\boldsymbol{\theta}} \tilde{u}$ is a $N_h \times N_\theta$ matrix, and $\sum_{r=1}^{N_R} (\epsilon_r/c_\epsilon) \mathbb{I}_r$ is a $1 \times N_h$ vector, whose elements are zero, except at N_R positions $\{j(r)\}_{r=1}^{N_R}$, corresponding to the N_R recording points. Then, the right-hand side in the above formula is a $1 \times N_\theta$ vector, whose i -th element reads $\sum_{r=1}^{N_R} (\epsilon_r/c_\epsilon) \sum_{m=0}^{N_t-1} \partial_{\boldsymbol{\theta}_i} \tilde{u}_{j(r)}(t_m, \boldsymbol{\theta}^*)$, with $i = 1, \dots, N_\theta$. The desired estimate follows, noting that $\sum_{m=0}^{N_t-1} |\partial_{\boldsymbol{\theta}_i} \tilde{u}_{j(r)}|$ is bounded from below and above away from zero, thanks to assumptions A1 and A2.

Appendix B.

In this appendix, we show that

$$\sum_{r=1}^{N_R} \sum_{m=0}^{N_t-1} \nabla_{\boldsymbol{\theta}} \nabla_{\boldsymbol{\theta}} \mathbf{g}_r(t_m, \boldsymbol{\theta}^*) \circ \mathbf{C}_\epsilon^{-1} \boldsymbol{\epsilon}_r = \mathcal{O}_P(N^{1/2}).$$

As in appendix A, we consider only the case when $d = 1$. We have

$$\nabla_{\boldsymbol{\theta}} \nabla_{\boldsymbol{\theta}} \mathbf{g}_r = \nabla_{\boldsymbol{\theta}} \left(\mathbb{I}_r \nabla_{\boldsymbol{\theta}} \tilde{u} \right) = \nabla_{\boldsymbol{\theta}} \nabla_{\boldsymbol{\theta}} \tilde{u} \circ \mathbb{I}_r^{\top},$$

where $\nabla_{\boldsymbol{\theta}} \nabla_{\boldsymbol{\theta}} \tilde{u}$ is a $N_{\theta} \times N_{\theta} \times N_h$ tensor. Note that for two real vectors, $\mathbf{a}, \mathbf{b} \in \mathbb{R}^p$, we use the notation $\nabla_{\boldsymbol{\theta}} \nabla_{\boldsymbol{\theta}} \mathbf{a} \circ \mathbf{b} = \sum_{i=1}^p b_i \nabla_{\boldsymbol{\theta}} \nabla_{\boldsymbol{\theta}} a_i$. Therefore, we have

$$\sum_{r=1}^{N_R} \sum_{m=0}^{N_t-1} \nabla_{\boldsymbol{\theta}} \nabla_{\boldsymbol{\theta}} \mathbf{g}_r(t_m, \boldsymbol{\theta}^*) \circ \mathbf{C}_{\epsilon}^{-1} \boldsymbol{\epsilon}_r = \sum_{m=0}^{N_t-1} \nabla_{\boldsymbol{\theta}} \nabla_{\boldsymbol{\theta}} \tilde{u}(t_m, \boldsymbol{\theta}^*) \circ \sum_{r=1}^{N_R} \mathbb{I}_r^{\top} \frac{\boldsymbol{\epsilon}_r}{c_{\epsilon}}.$$

Similar to Appendix A, we can show that the right hand side in the above formula is a $N_{\theta} \times N_{\theta}$ matrix whose element (i, k) reads $\sum_{r=1}^{N_R} (\epsilon_r / c_{\epsilon}) \sum_{m=0}^{N_t-1} \partial_{\boldsymbol{\theta}_i}^2 \tilde{u}_{j(r)}(t_m, \boldsymbol{\theta}^*)$. The desired estimate follows, noting that $\sum_{m=0}^{N_t-1} \partial_{\boldsymbol{\theta}_i}^2 \tilde{u}_{j(r)}$ is bounded from below and above away from zero, thanks to assumptions A1 and A2.

Appendix C.

In this appendix, we show that

$$\sum_{r=1}^{N_R} \sum_{m=0}^{N_t-1} \nabla_{\boldsymbol{\theta}} \mathbf{g}_r(t_m, \boldsymbol{\theta}^*)^{\top} \mathbf{C}_{\epsilon}^{-1} \nabla_{\boldsymbol{\theta}} \mathbf{g}_r(t_m, \boldsymbol{\theta}^*) = \mathcal{O}(N).$$

Again, we consider only the case when $d = 1$. Since $\nabla_{\boldsymbol{\theta}} \mathbf{g}_r = \mathbb{I}_r \nabla_{\boldsymbol{\theta}} \tilde{u}$, we have

$$\sum_{r=1}^R \sum_{m=0}^{N_t-1} \nabla_{\boldsymbol{\theta}} \mathbf{g}_r(t_m, \boldsymbol{\theta}^*)^{\top} \mathbf{C}_{\epsilon}^{-1} \nabla_{\boldsymbol{\theta}} \mathbf{g}_r(t_m, \boldsymbol{\theta}^*) = c_{\epsilon}^{-1} \sum_{m=0}^{N_t-1} \nabla_{\boldsymbol{\theta}} \tilde{u}(t_m, \boldsymbol{\theta}^*)^{\top} \sum_{r=1}^{N_R} \mathbb{I}_r^{\top} \mathbb{I}_r \nabla_{\boldsymbol{\theta}} \tilde{u}(t_m, \boldsymbol{\theta}^*).$$

We note that $\sum_{r=1}^{N_R} \mathbb{I}_r^{\top} \mathbb{I}_r$ is a diagonal $N_h \times N_h$ matrix whose diagonal elements are zeros, except elements $\{(j(r), j(r))\}_{r=1}^{N_R}$, which are 1's. Therefore, the right-hand side in the above formula is a $N_{\theta} \times N_{\theta}$ matrix whose element (i, k) reads $c_{\epsilon}^{-1} \sum_{r=1}^{N_R} \sum_{m=0}^{N_t-1} \partial_{\boldsymbol{\theta}_i} \tilde{u}_{j(r)} \partial_{\boldsymbol{\theta}_k} \tilde{u}_{j(r)}$. The desired estimate follows, noting that $\sum_{m=0}^{N_t-1} |\partial_{\boldsymbol{\theta}_i} \tilde{u}_{j(r)} \partial_{\boldsymbol{\theta}_k} \tilde{u}_{j(r)}|$ is bounded from below and above away from zero, thanks to assumptions A1 and A2.

Reference

References

- [1] J. Bäck, F. Nobile, L. Tamellini, and R. Tempone. Stochastic spectral Galerkin and collocation methods for PDEs with random coefficients: a numerical comparison. In J. S. Hesthaven and E.M. Ronquist, editors, *Spectral and High Order Methods for Partial Differential Equations. Lecture Notes in Computational Science and Engineering*, volume 76, pages 43–62. Springer, 2011.
- [2] V. Barthelmann, E. Novak, and K. Ritter. High dimensional polynomial interpolation on sparse grids. *Advances in Computational Mathematics*, 12(4):273–288, 2000.

- [3] J. Beck, F. Nobile, L. Tamellini, and R. Tempone. On the optimal polynomial approximation of stochastic PDEs by Galerkin and collocation methods. *Mathematical Models and Methods in Applied Sciences*, 22:1250023–1–1250023–33, 2012.
- [4] K. Chaloner and I. Verdinelli. Bayesian experimental design: a review. *Statistical Science*, 10(3):273–304, 1995.
- [5] R. Clayton and B. Engquist. Absorbing boundary conditions for acoustic and elastic wave equations. *Bulletin of the Seismological Society of America*, 67:1529–1540, 1977.
- [6] S. M. Day, J. Bielak, D. Dreger, S. Larsen, R. Graves, A. Ptarka, and K. B. Olsen. Tests of 3D elastodynamic codes: Lifelines program task 1A01. Technical report, Pacific Earthquake Engineering Center, 2001.
- [7] M. B. Giles. Multilevel monte carlo path simulation. *Operations Research*, 56(3):607–617, 2008.
- [8] W. W. Hager. Updating the inverse of a matrix. *SIAM Review*, 31(2):pp. 221–239, 1989.
- [9] A.-L. Haji-Ali, F. Nobile, and R. Tempone. Multi Index Monte Carlo: When Sparsity Meets Sampling. *ArXiv e-prints*, May 2014.
- [10] X. Huan and Y. M. Marzouk. Simulation-based optimal bayesian experimental design for nonlinear systems. *Journal of Computational Physics*, 232(1):288 – 317, 2013.
- [11] S. Kullback and R. A. Leibler. On information and sufficiency. *The Annals of Mathematical Statistics*, 22(1):pp. 79–86, 1951.
- [12] Q. Long, M. Scavino, R. Tempone, and S. Wang. Fast estimation of expected information gains for Bayesian experimental designs based on Laplace approximation. *Computer Methods in Applied Mechanics and Engineering*, 259:24–39, 2013.
- [13] Q. Long, M. Scavino, R. Tempone, and S. Wang. A Laplace method for under-determined Bayesian optimal experimental design. *Computer Methods in Applied Mechanics and Engineering*, 285:849–876, 2015.
- [14] M. Motamed, F. Nobile, and R. Tempone. Analysis and computation of the elastic wave equation with random coefficients. MATHICSE Technical Report 32.2012, EPFL, Switzerland, 2012.
- [15] M. Motamed, F. Nobile, and R. Tempone. A stochastic collocation method for the second order wave equation with a discontinuous random speed. *Numerische Mathematik*, 123:493–536, 2013.
- [16] S. Nilsson, N. A. Petersson, B. Sjögren, and H.-O. Kreiss. Stable difference approximations for the elastic wave equation in second order formulation. *SIAM Journal on Numerical Analysis*, 45:1902–1936, 2007.
- [17] F. Nobile, R. Tempone, and C. G. Webster. A sparse grid stochastic collocation method for partial differential equations with random input data. *SIAM Journal on Numerical Analysis*, 46(5):2309–2345, 2008.
- [18] E. Novak and K. Ritter. The curse of dimension and a universal method for numerical integration. In G. Nürnberger, J. W. Schmidt, and G. Walz, editors, *Multivariate Approximation and Splines*, pages 177–188. Birkhäuser, Basel, 1997.
- [19] N. A. Petersson and B. Sjögreen. An energy absorbing far-field boundary condition for the elastic wave equation. *Communications in Computational Physics*, 6:483–508, 2009.
- [20] K. J. Ryan. Estimating expected information gains for experimental designs with application to the random fatigue-limit model. *Journal of Computational and Graphical Statistics*, 12(3):585–603, 2003.
- [21] B. Sjögreen and N. A. Petersson. Source estimation by full wave form inversion. *Journal of Scientific Computing*, 59:247–276, 2014.
- [22] S. A. Smolyak. Quadrature and interpolation formulas for tensor products of certain classes of functions. *Doklady Akademii Nauk SSSR*, 4:240–243, 1963.
- [23] A. M. Stuart. Inverse problems: A Bayesian perspective. *Acta Numerica*, 19:451–559, 2010.
- [24] J. Virieux and S. Operto. An overview of full-waveform inversion in exploration geophysics. *Geophysics*, 74:WCC1–WCC26, 2009.